Global and Planetary Change 188 (2020) 103153

Contents lists available at ScienceDirect

Global and Planetary Change

journal homepage: www.elsevier.com/locate/gloplacha

Research article

Photic-zone euxinia and anoxic events in a Middle-Late Devonian shelfal sea of Panthalassan continental margin, NW Canada: Changing paradigm of Devonian ocean and sea level fluctuations

P. Kabanov*, C. Jiang

Geological Survey of Canada Calgary, Calgary, AB T2L 2A7, Canada

ARTICLE INFO

Keywords:
Mid-Devonian to Frasnian
Black shales
Chemostratigraphy
Anoxic events
Biomarkers
Hyalosponge spicules
Photic zone euxinia
Greenhouse ocean

ABSTRACT

The latest Eifelian – Frasnian strata of the Mackenzie Valley, NW Canada, provide an excellent archive of paleoceanographic signals imprinted in oxic and anoxic facies deposited in close proximity. Fondoformic black-shale strata preserve fingerprints of four global anoxic events (Kačák, Frasnes, Middlesex, and Rhinestreet), which receives confirmation with $\delta^{13}C_{org}$ data. The discovery of 2,3,6- and 3,4,5-trimethyl aryl isoprenoids (biomarkers of green sulfur bacteria) at and between the levels of anoxic events contributes to the growing evidence of photic-zone euxinia as a common state of oceanographically open and semi-restricted shelfal basins of the Middle Devonian – Early Mississippian; a condition impossible under present-day vigorous thermohaline circulation, but consistent with models of greenhouse ocean depicting drastic slowdown in watermass turnover, reversals of deep ocean circulation, greatly expanded oxygen minimum zones, and profoundly changed nutrient flows. The rocks under study were deposited in an oceanographically open basin with fluctuating chemocline as attested by unstable presence of gammacerane in GCMS spectra and co-occurrence of signatures of water-column euxinia and pyritized hyalosponge spicules indicating episodes of weak bottom oxygenation. Shallow-water carbonate banks in the same basin show signatures of reduced hydrodynamic activity and do not record sea level changes in excess of several meters, which lines up with the shortage of evidence for high-amplitude base-level fluctuations in coeval strata worldwide. This supports discarding changes in sea level as the principal control over Devonian anoxic events and instead suggests pulsatory expansions of thick, semi-continuous oxygen minimum zones of the greenhouse ocean. Sea level fluctuations could still be involved as non-glacial (thermal and aquifer?) eustatic transgressions of a very modest amplitude.

1. Introduction

The second half of the Devonian (~388–359 My) is marked by spread of anoxic/dysoxic fine-grained sediments (a.k.a. black shales) in many shelfal basins of the World (Fig. 1; Falkowski et al., 2011; Kabanov, 2019). This period of anoxic shelfal sedimentation protracted into the Lower Mississippian to comprise one of six Phanerozoic time bins of major source rock deposition (Klemme and Ulmishek, 1991). In Devonian-Mississippian sedimentary systems, black shales commonly associate with isolated carbonate banks (reefs, pinnacles, mud mounds) outposting carbonate shelves far into the basin (Playford, 1980; Stoakes, 1980; Meijer Drees, 1993; Stanton et al., 2000; Gatovskii et al., 2016; Knapp et al., 2017; Kabanov and Gouwy, 2017). Major sea level fluctuations have been proposed to temporally separate depositional phases of carbonate buildups and basinal sediments (Jewell, 1994; House et al., 2000) and accommodate the evidence of hydrodynamic disturbance in black shales and their stratigraphic juxtaposition with oxic, apparently shallow-water fossiliferous facies (Brett et al., 2011; Knapp et al., 2017). However, debate seems to be everlasting in the shortage of rigorous evidence of eustatic fluctuations (Ettensohn, 1994; Hallam and Wignall, 1999; Bond and Wignall, 2008; Smith et al., 2019, 2020; Ver Straeten et al., 2020).

Global and local processes beyond this clearly non-actualistic condition of shelfal seas are poorly understood except for their strong causal relation with the greenhouse state of our planet (Algeo and Scheckler, 1998; Racki, 2005; Bond and Grasby, 2017; Carmichael et al., 2019; Percival et al., 2020). Most substantiated models involve atmosphere/ocean systems maintained in warm-greenhouse mode by successive and/or combined degassing in Vilyui, Dnieper-Donets, and Kola continental large igneous provinces (LIPs), as well as in a number

* Corresponding author.
E-mail address: Pavel.Kabanov@canada.ca (P. Kabanov).

https://doi.org/10.1016/j.gloplacha.2020.103153
Received 24 December 2019; Received in revised form 25 February 2020; Accepted 28 February 2020
Available online 05 March 2020

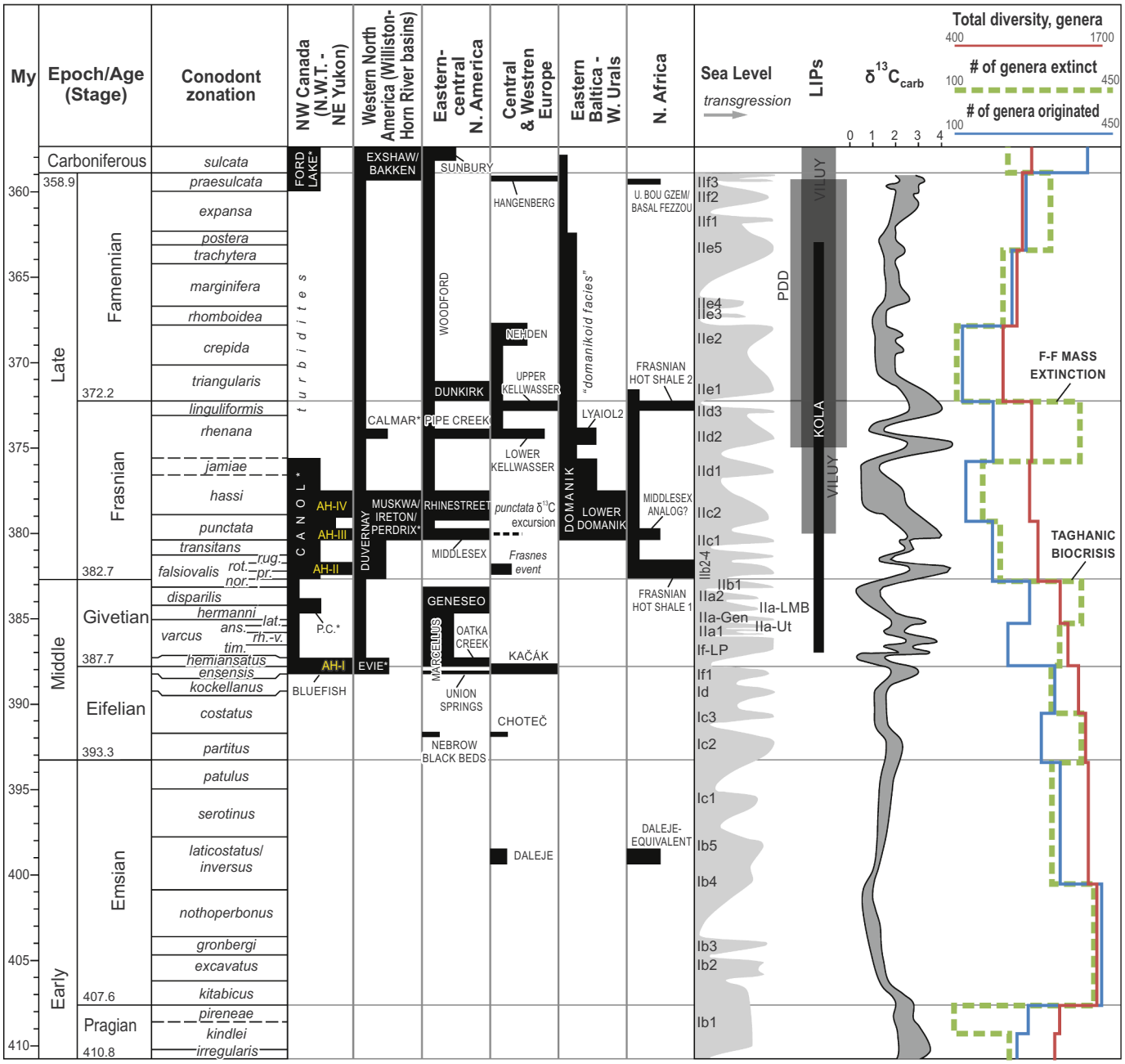

Fig. 1. Occurrence of black shales in six global regions in the post-Lochkovian Devonian plotted against sea level curve under discussion (redrawn from Becker et al., 2016), $\delta^{13}C$ (‰, VPDB) curve from skeletal carbonate (Saltzman and Thomas, 2012; Becker et al., 2012), extinction-origination curves for marine fauna (Paleobiology Database; supplementary materials of Melott and Bambach, 2014), and age ranges of Large Igneous Provinces (LIPs); modified from Kabanov (2019). Width of LIP bars represents relative volumes of emplaced effusives without differentiation between eruption pulses; their ages are updated based on the compilation of Racki (2020). Calibration of radiometric ages from Geologic Time Scale 2012 (Becker et al., 2012)); these ages stay unchanged as of 2018 (Cohen et al., 2013, updated on 2018). Alternative conodont zones in Givetian-Frasnian (Narkiewicz and Bultynck, 2007; Becker et al., 2016): *tim.* = *timorensis, rh.-v.* = *rhenanus-varcus, ans.* = *ansatus, lat.* = *latifossatus/semialternans, nor.* = *norrisi, pr.* = *pristina, rot.* = *rotundiloba, rug.* = *rugosa.* Depophase indexing in the sea level curve is retained from Johnson et al. (1985). Sources for chronostratigraphic position of anoxic shales and age ranges of LIPs are given in Kabanov (2019). Block length in LIPs denote oldest and youngest absolute ages, and width reflects relative volume of emplaced basalts; PDD is Pripyat'-Dnieper-Donets Rifted Basin. Labelled in yellow are anoxic horizons (AHs) of the Horn River Group. (P.C.) is yet another possible horizon of enhanced anoxia in the middle of Prohibition Creek Member of the Hare Indian Formation (see text). Asterisks denote black shales with notably poor age constraints of their bases or tops. (For interpretation of the references to colour in this figure legend, the reader is referred to the web version of this article.)

of smaller continental magmatic centers and volcanic arcs (Fig. 1: Kidder and Worsley, 2010; Kravchinsky, 2012; Bond and Wignall, 2014; Ernst et al., 2020; Racki, 2020), which gains support in the evidence that Kellwasser anoxic events and the collapse of marine ecosystems at the Frasnian-Famennian boundary associate with bursts of effusive activity (Racki et al., 2018). An alternative explanation links the spreads of shelfal anoxia to the "top-down" eutrophication of shelfal seas caused by the erosion of soils which during the second half of the Devonian experienced dramatic expansion due to land afforestation (Algeo et al., 1995; Algeo and Scheckler, 1998; Carmichael et al., 2016, 2019; Percival et al., 2019), which, however, does not find support in paleosol and paleobotanical research (Retallack and Huang, 2011).

Table 1
Selected reports of PZE biomarkers in Middle Devonian – Lower Mississippian black shales.

Case study	Age range of samples	Lithostratigraphy	Basin	major biotic extinction	PZE biomarkers	Oceanographic regime of the basin
This study	Latest Eifelian - M. Frasnian[1]	Horn River Group (Canol, Bluefish)	Peel Shelf, Canada	None	trimethyl aryl isoprenoids; isorenieratane	Open[1]
Jiang et al. (2001), Aderoju and Bend (2018)	E. Famennian - L. Tournaisian[2]	Bakken Fm.	Williston Basin, Canada	None (D/C)	aryl isoprenoids; isorenieratane, paleorenieratane	Open to semi-restricted[3]
Spaak et al. (2018)	L. Givetian - L. Frasnian[4]	Gogo Fm.	Canning Basin, Australia	None (?LG)	chlorobactane, isorenieratane, paleorenieratane	Semi-restricted[5]
Bushnev et al. (2016)	Middle Frasnian[10]	Domanik Fm.	Timan-Pechora Basin, Russia	None	isorenieratane, β-isorenieratane	NED
Brown and Kenig (2004)	L. Givetian - E. Mississippian	New Albany Fm., Antrim Fm.	Michigan and Illinois basins, U.S.A.	F/F (LG; D/C)	isorenieratane; C_{40} diaryl isoprenoid (compound X)	Semi-restricted[3]
Joachimski et al. (2001)	L. Frasnian - E. Famennian[6]	Organic rich shales and carbonates of Lower and Upper Kellwasser black shales	Holy Cross Mts., Poland	F/F	Isorenieratane; diaryl isoprenoids	NED; carbonate-shelf facies interbedded with black shales[6]
Marynowski et al. (2008)	M. Frasnian	Organic rich shales and carbonates equivalent to Rhinestreet and Middlesex sourcerocks	Holy Cross Mts., Poland	None	Isorenieratane; diaryl isoprenoids	*Ibid.*
Marynowski and Filipiak (2007), Marynowski et al. (2012)	L. Famennian - E. Touraisian	Organic rich shales equivalent to Hangenberg black shale	Holy Cross Mts., Poland	None (D/C)	isorenieratane; aryl isoprenoids	*Ibid.*
Connock et al. (2018)	E. Frasnian-E. Tournaisian	Woodford Fm.	Arkoma Basin, U.S.A.	F/F (?D/C)	paleorenieratane, isorenieratane, renierapurpurane	Open to semi-restricted[3]
Requejo et al. (1992)	E.-M. Frasnian[9]	Duvernay Fm.	Western Canada Sedimentary Basin	None	Aryl isoprenoids; isorenieratane	NED
Riboulleau et al. (2018)	L. Frasnian - Famennian	Aouinet Ouenine Fm., units III and IV	Ghadames Basin, Libya	NED;? F/F	palaerenieratane; isorenieratane; aryl isoprenoids	NED; likely semi-restriced[8]
Haddad et al. (2016)	L. Frasnian-E.Famennian[11]	Tomachi Fm., Upper Kellwasser equiv. interval	Madre de Dios Basin, Bolivia	F/F	trace isorenieratane and palaerenieratane; no isorenieratane at F/F level	NED
Haddad et al. (2016)	L. Frasnian-E.Famennian[3]	Hannover Fm., Upper Kellwasser equiv. interval	Appalachian Basin, U.S.A.	F/F	low abundance of aryl isoprenoids and palaerenieratane; trace isorenieratane	Semi-restricted[3]
Philp and DeGarmo (2020)	Givetian-Famennian[12]	Woodford Fm.	Oklahoma Basin, U.S.A.	NED	trimethyl aryl isoprenoids; isorenieratane	Open[3]

Note: Records from related oils are omitted. The Givetian-Lower Mississippian includes one major biotic extinction at the Frasnian-Famennian boundary (F/F). Minor biotic perturbations are parenthesized: (LG) Late Givetian extinction and (D/C) Devonian/Carboniferous boundary turnover. NED = not enough data. References to geologic age and paleoceanographic settings: [1]Kabanov (2019); [2]Johnston et al., (2010); [3]Algeo and Tribovillard (2009); [4]Nicoll, (1984); [5]Spaak et al. (2018); [6]Narkiewicz (2007); [8]Riboulleau et al. (2018); [9]Wendte and Uyeno (2005); [10]Gatovskii et al. (2016); [11]Haddad et al. (2016); [12]Philp and DeGarmo (2020).

Noteworthy, the known absolute ages of effusives in the Devonian continental LIPs are younger than the mid-Devonian (latest Eifelian) onset of widespread black shale sedimentation (Fig. 1), which is probably accounted for the incompleteness of absolute age records (Bond and Wignall, 2014; Ernst et al., 2020). This mid-Devonian shift in global condition is referred to as the Kačák or Kačák-*otomari* Event (House, 1996; Van Hengstum and Gröcke, 2008).

Extreme spreads of anoxic facies have been correlated globally as the Devonian black shale or anoxic events (House, 1983, 2002; Sandberg et al., 2002; Bond et al., 2004; Racki, 2005; Becker et al., 2016). Some, but not all, of these black shale events are coupled with biotic perturbations (Fig. 1) ranked as major in ecological severity (McGhee Jr. et al., 2013) and minor or moderate except for the Frasnian/Famennian in net taxonomic loss (Melott and Bambach, 2014). Basins where Devonian anoxic events are well-documented include those with signatures of impeded watermass exchange and those with evidence of oceanographic openness (Table 1; Carmichael et al., 2019). In the Devonian eustatic sea-level curve of Johnson et al. (1985) and its later modifications, anoxic horizons are seen as a result of genuine deepening or global transgressions (Sandberg et al., 2002; Arthur and Sageman, 2005; Ver Straeten et al., 2011; Brett et al., 2011), and this sea-level curve is the most common reference in case studies today (*e.g.,* Pyle and Gal, 2016; Fraser and Hutchison, 2017; Dong et al., 2018; Philp and DeGarmo, 2020).

On the other hand, insights into the nature of the Middle Paleozoic anoxic events indicate possible links with profound change of circulation pattern and expansion of oxygen minimum zones (OMZs) of the ocean into shallower depth (Meyer and Kump, 2008), which is consistent with extensive biomarker evidence of photic-zone euxinia (PZE) at and between the stratigraphic levels of Middle Paleozoic biotic perturbations (Table 1 and references therein). In should be noted that the idea of oceanic circulation reversal as a critical component of the greenhouse planetary condition had century-long incubation period, but only recently growing knowledge pushed it into mainstream science (Hay and Floegel, 2012). Here we report more evidence from a Panthalassa-facing shelfal sedimentary system and contend that factors other than sea level rise controlled the spreads of black shales in Middle Paleozoic shelfal seas.

2. Geologic and palaeogeographic context

The study area is situated in the northwestern part of the Ancestral North America (ANA; Fig. 2A). The ANA refers to the main part of Laurentia as opposed to cordilleran terranes accreted during Meso-Cenozoic (Gabrielse and Yorath, 1991; Nelson et al., 2013). The Peel Platform (a.k.a. Peel Shelf, Mackenzie or Mackenzie-Peel Platform) refers to the Lower Paleozoic – Eifelian shallow-water carbonates of the northwestern ANA (Fallas et al., in press). The Peel Platform is bordered from the west by the Richardson and Selwyn shale basins (Fig. 2A) and from the east by the erosional truncation towards the Laurentian Shield. The Hume limestone in the top of the Peel Platform succession is onlapped with the geographically extensive drowning unconformity (*sensu* Schlager, 1989) by the basal black shale unit of the Horn River Group (HRG) called Bluefish Member (Kabanov and Gouwy, 2017; Kabanov, in press).

The HRG occurs in the Laramide cordillera and in the subsurface of adjacent interior plains of Northwest Territories (Fig. 2B) and is composed of the Hare Indian, Ramparts, and Canol formations (Fig. 2C). The most accurate age brackets available to date are provided by conodonts (Fig. 1B; data of S. Gouwy reviewed by Kabanov, 2019; Gouwy, in press). The occurrence of thick (150–400 m) Hare Indian and Ramparts strata defines the BAT (bank-and-trough) palaeogeographic area (Fig. 2B,C; Kabanov and Deblonde, 2019). The Bell Creek Member is a thick (up to 190 m) succession of grey, variously calcareous shales and siltstones with a mixture of benthic and pelagic fossils overlying the Bluefish Member and representing clinoformic basin fills or "deltaic shale lobes" prograded from the easterly located Laurentian landmass (Muir and Dixon, 1985; Kabanov et al., 2016a). The Ramparts Formation is composed of three main parts (Gal et al., 2009) and is best described as carbonate banks (Yose et al., 2001) outgrowing thick shale lobes of the Hare Indian Formation (Fig. 1B). The informal lower platform member refers to an argillaceous and silty limestone overlying, and partly intergrading with, the upper Bell Creek. The Carcajou unit is a thin (< 3.0 m) limestone with benthic fauna distinguished by its dark argillaceous matrix and elevated gamma-ray response. The Kee Scarp Member is a portion of the Ramparts Formation developed above the Carcajou as spatially restricted carbonate banks (Gal et al., 2009). In the best studied example from Norman Wells oilfield, the Kee Scarp reveals the backstepped stacking pattern of subtidal-intertidal parasequences (Yose et al., 2001). Some carbonate banks are aproned by thin (0.1–6.0 m) "allochthonous limestones" composed of graded laminated calcisiltites and calcarenites interbedded with Canol shales (Mackenzie, 1973; Pugh, 1983).

The Canol Formation is the main prospect for shale hydrocarbons in the region (AANDC, 2014; Pyle and Gal, 2016; Kabanov and Gouwy, 2017). It is composed of laminated siliceous pyritic shale, pelagic (radiolaria-rich) chert, and minor siltstone, authigenic limestone and dolomite (Pyle and Gal, 2016; Kabanov and Gouwy, 2017). The Canol Formation is mostly thin (<20 m) in BAT and disappears on tops of tallest carbonate banks intersected by wells (Fig. 1B; Pugh, 1983; Kabanov and Deblonde, 2019), but just south of Norman Wells it thickens to 60–120 m while the Hare Indian Formation thins inversely into a black shale dominated package. Kabanov and Gouwy (2017) named this paleogeographic zone *the southern off-bank area* (SOB), and it is where the sections discussed in this paper are located (Fig. 2B). The western off-bank area (WOB) is defined by similar thickening of the Canol Formation and inverse thinning of the Hare Indian Formation to the west of 130° meridian. Further west, across 132°N, the entire Hare Indian Formation is considered merging into the Canol Formation as its gamma and resistivity log signatures disappear in response to attenuation of siliciclastic components (Kabanov and Deblonde, 2019; Kabanov, in press). In off-bank areas, the HRG is fondoformic (*sensu* Rich, 1951), and its superficially monotonous black shale lithology impedes its subdivision with conventional observations justifying usage of the "Horn River Group undivided" map unit (Fallas and MacNaughton, 2013, 2019). In the lithostratigraphy of these fondoformic strata proposed by Kabanov and Gouwy (2017) for the SOB area, subdivision of the HRG and the basal Imperial shales heavily relies on well logs and gamma spectrometry surveys of outcrops, but lithologic observations of cores and outcrops are also entered in definition of lithostratigraphic units. This lithostratigraphy is now carried over to WOB area (Kabanov and Deblonde, 2019; Kabanov, in press) and used in this work (Figs. 2C, 3, and 5).

The Canol Formation grades upward into the fine clinoformic siliciclastics of the Imperial Formation. These siliciclastics deposited in the Ellesmerian foreland setting encroached from the present-day North by early Late Frasnian, Laurentia remained the main sourceland for the study area during the Imperial deposition (Lane, 2007; Hadlari et al., 2009; Beranek et al., 2010). In this paper, the basal Imperial is an informal reference to the grey and dark shales of the Mirror Lake and Loon Creek members between the top of Canol Formation and the base of the Canyon Member (Figs. 2C and 3).

2.1. Terminology note: usage of "fondoformic strata"

Rich (1951) introduced the terms clinoform, undaform, and fondoform to describe three critical depositional environments, which were the generalizing expansions of the deltaic foreset, topset, and bottomset, correspondingly. Only the first of this triade is universally used in the geological lexicon today owing to its expansion to the entire sigmoid, including the bottomset and the topset, in the mainstream seismic and sequence stratigraphy (Steel and Olsen, 2002; Patruno and

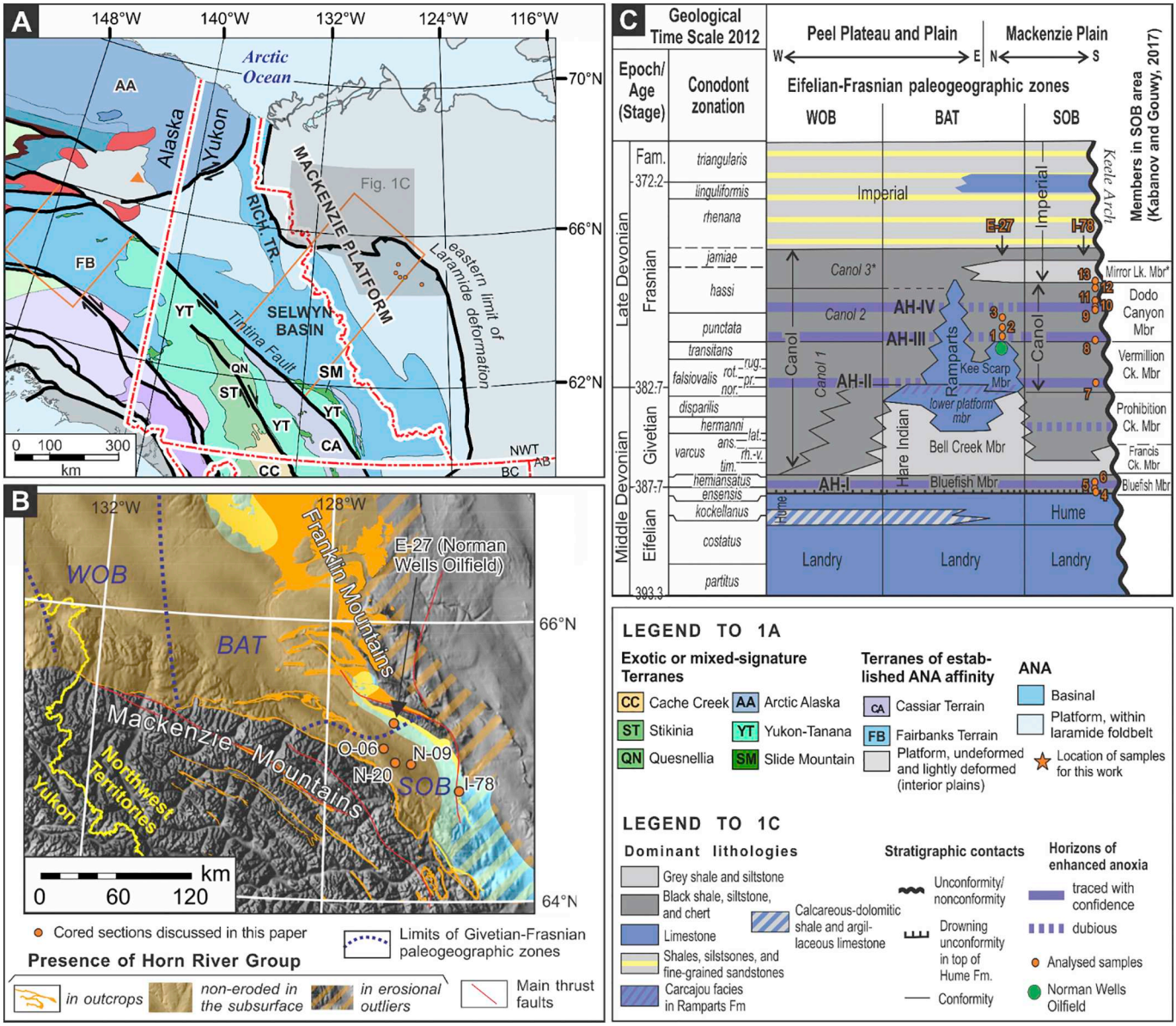

Fig. 2. Structural, paleogeographic, and stratigraphic context. Orange circles on (A) and (B) are wells appearing in this paper: (I-78) East Mackay I-78, (E-27) Mackenzie River # 4 (E-27), (O-09) Little Bear N-09, (N-20) Mirror Lake N-20, and (O-06) Loon Creek O-06. **(A)** Map of cordilleran terranes (adapted from GIS project in Colpron and Nelson, 2011). Basinal and platformal areas of the Ancestral North America (ANA) are adapted to Devonian paleogeography. The shaded area is assessed by the stratigraphic chart on part figure (C). Rich.Tr. = Richardson Trough. Torn orange rectangle denotes approximate restored paleogeographic profile on Fig. 7. **(B)** Givetian-Frasnian paleogeographic zones and HRG occurrence in outcrops and the subsurface; highlighted are zones of low thermal maturity yielding samples for biomarker study (based on data in Pyle et al., 2015 and Kabanov, 2017); basemap is the enhanced topographic model. Paleogeographic zones: WOB = western off-bank, BAT = bank and trough, SOB = southern off-bank. **(C)** The Eifelian-Frasnian chronostratigraphic chart (modified from Kabanov and Deblonde, 2019), horizons of enhanced anoxia (Kabanov et al., 2019), and position of samples for biomarker study. Conodont zonation is based on summary and new data of S.A. Gouwy (reviewed in Kabanov, 2019). Samples in reference to measured core depth (m) in Mackenzie River # 4 (E-27): (1) 403.34; (2) 402.67; (3) blended samples from 399.00, 398.66, 398.33, and 398.00 m. In East MacKay I-78: (4) 1956.5; (5) 1953.0; (6) 1944.00; (7) 1873.00; (8) 1855.00; (9) 1844.00; (10) 1841.00; (11) 1831; (12) 1824.00; and (13) 1820.00. See Jiang et al. (2020) for more information on biomarker study samples.

Helland-Hansen, 2018). This approach, however, is too simplistic and depraves sedimentary blankets of basin floors in their own right. Basinal sediments are often dominated by pelagic material and possess stratigraphic architecture unrelated to siliciclastic provenance. We are not alone who reinstate undeservedly neglected usage of Rich's (1951) "fondoform" (*e.g.,* Schlager, 2005), and the same rationale likely applies to the concept of undaform (Schlager, 2005).

3. Samples and methods

This paper reports on new organic geochemistry and stable organic-carbon isotope results from diamond-drill cores and sums up observations on the stratigraphic distribution of sponge spicules. Supplementary materials for this paper include stable carbon isotope data of organic matter ($\delta^{13}C_{org}$, ‰ VPDB notation) and their acquisition protocols, as well as SEM and light-microscope identification of sponge spicules and character of their pyritization.

3.1. Organic geochemistry samples

The organic geochemistry samples were obtained from Mackenzie River E-27 and East MacKay I-78 wells located in the relatively low-

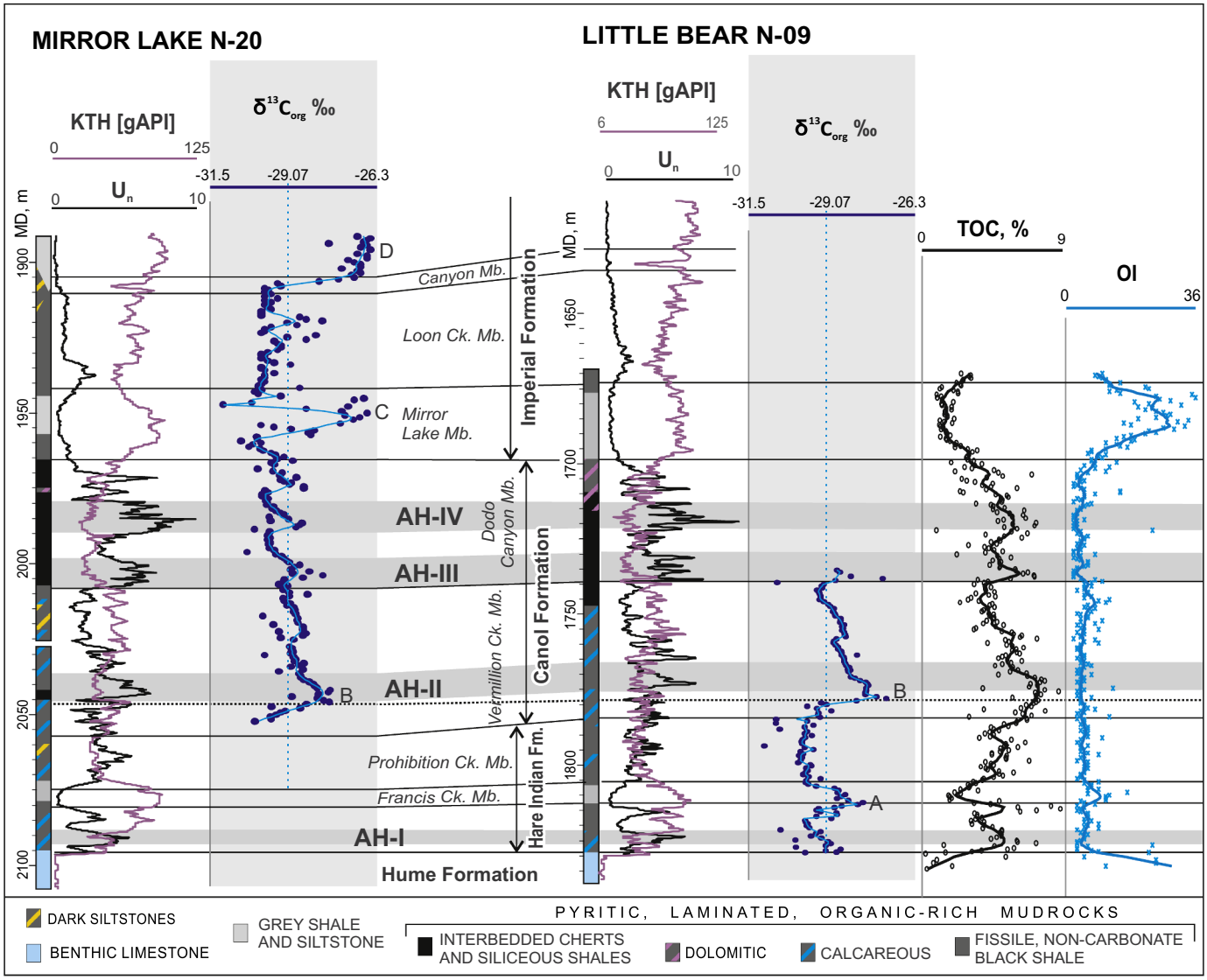

Fig. 3. Two cored sections of the HRG and the basal Imperial Formation in SOB area. Each section is characterized with gamma spectrometry proxies KTH and U_n from geophysical spectralogs and $\delta^{13}C_{org}$. The Rock-Eval pyrolysis parameters TOC and OI are available for Little Bear N-09 well only. Dotted vertical line is the $\delta^{13}C_{org}$ median for the HRG in both wells. Curves on $\delta^{13}C_{org}$, TOC, and OI cross-plots are LOWESS regression lines with α-tension 4%. Data points for $\delta^{13}C_{org}$ and OI are truncated at 0.95 percentile. Legend at the bottom decodes observed core lithology in simplified form.

maturity (oil window) zone (Figs. 2B,C; Table 2). Selection of less mature sections was critical as samples from the adjacent area of more advanced thermal maturity showed correspondingly advanced elimination of indigenous organic compounds (Jiang et al., 2020). Powdered shale rock samples have been subjected to solvent extraction, open column chromatographic separation and gas chromatography–mass spectrometry (GC–MS) analyses as briefly described below. Samples for biomarkers were taken from 1 to 2 cm thick stratigraphic intervals where they incorporate many individual sedimentary laminae which typically range in thickness from 0.1 to 1.0 mm.

3.2. Solvent extraction and column chromatographic separation

Five to 20 g of powdered rock from each sample was subjected to Soxhlet extraction for 72 h using dichloromethane as solvent. Activated copper grains were added to the extract content at the end of extraction to remove any elemental sulfur. After removing most of solvent using a rotary evaporator, the extract contents were filtered to remove copper, copper sulfide and any other solids. The residue was retained and weighed as total extracts after removal of the remaining solvent using a gentle stream of nitrogen.

Rock extracts were de-asphaltened with *n*-pentane and then separated into saturated, aromatic and resin fractions by column chromatography using a mixture of silica gel and alumina (1:3 by weight) as support. *n*-Pentane (3.5 mL per gram of support) was used to elute the aliphatic fraction, followed by *n*-pentane/dichloromethane (1:1 by volume and 4 mL per gram of support) to isolate the aromatic fraction. Methanol (4 mL per gram of support) and chloroform (6 mL per gram of support) were finally used to obtain the resin fraction.

3.3. GC and GC–MS analysis of saturated and aromatic fractions

GC analysis of saturated fractions was completed on a Varian 3700 GC equipped with a flame ionization detector (FID). A 30 m × 0.25 mm × 0.25 μm DB-1 fused silica capillary column was used with helium as carrier gas. The samples were injected using a split injector heated to 320 °C. The temperature program was as follows: 60 °C (at 6 °C/min) → 300 °C (30 min). The FID temperature was maintained at 320 °C.

GC–MS analysis of saturated fractions was carried out on an Agilent

Table 2
Organic geochemical parameters indicating thermal maturity and depositional environments for the Canol and Bluefish samples in this study.

Depth (m)	Stratum	Pr/Ph	C29H/C30H	Ts/Tm	C23T/C30H	C24Tet/C26T	C29St/C30H	Gamma/C30H	Steranes (%) Distribution			C29 St: S/(S + R)	C32H S/(S + R)	DBT/Phen	C18 TAI/AB	Trimethyl aryl isoprenoids		
									C27	C28	C29					C_{18}	C_{13}-C_{22}	C_{15}-C_{31}
1820	Canol-Imperial	1.55	0.35	2.62	0.43	0.22	0.64	0.07	38.6	14.9	46.5	0.53	0.60	0.13	15.11	379	n.a.	n.a.
1824	Canol-Imperial	1.69	0.45	1.92	0.70	0.20	0.65	0.05	38.4	16.0	45.6	0.54	0.61	0.14	34.44	417	n.a.	n.a.
1831	Canol	1.54	0.39	2.39	0.53	0.17	0.69	0.06	34.7	15.7	49.5	0.54	0.59	0.19	36.11	605	n.a.	n.a.
1841	Canol	1.27	0.60	1.22	0.85	0.20	0.78	0.07	35.7	17.8	46.6	0.53	0.61	0.30	32.32	575	333	363
1844	Canol	1.32	0.64	1.06	0.88	0.25	0.75	0.10	36.7	18.2	45.1	0.52	0.61	0.32	40.29	1367	481	471
1855	Canol	1.36	0.63	1.20	0.98	0.23	0.68	0.11	36.4	18.0	45.6	0.51	0.60	0.25	32.01	968	240	237
1873	Canol	1.21	0.62	1.77	1.00	0.20	0.90	0.10	37.2	16.3	46.4	0.53	0.61	0.30	82.52	872	414	412
1944	Bluefish	1.28	0.40	6.63	3.25	0.19	4.12	0.16	37.0	15.1	47.9	0.51	0.58	0.37	10.89	261	n.a.	n.a.
1953	Bluefish	1.18	0.40	9.80	2.83	0.17	3.04	0.23	34.5	15.5	50.0	0.52	0.62	0.33	11.00	237	130	138
1956.5	Bluefish	1.30	0.40	5.20	3.02	0.26	3.23	0.21	38.0	16.2	45.8	0.51	0.59	0.43	8.95	347	n.a.	n.a.
398	Canol	1.42	0.66	0.37	0.67	0.33	1.10	0.14	36.9	15.9	47.3	0.50	0.61	0.35	26.85	629	n.a.	n.a.
402.67	Canol	1.42	0.71	0.48	0.70	0.31	1.13	0.10	35.5	17.4	47.2	0.50	0.60	0.35	14.03	728	578	485
403.34	Canol	1.83	0.78	0.50	0.86	0.44	1.16	0.11	37.5	17.2	45.4	0.50	0.60	0.27	12.41	863	360	253

Note: Pr/Ph, Pr/nC17, Ph/nC18: ratios among pristane, phytane, and C_{17} and C_{18} n-alkanes; C29H/C30H: C_{29} over C_{30} hopanes ratio; Ts/Tm: 18α-22,29,30-trisnorneohopane over 17α-22,29,30-trisnorhopane; C23T/C30H: C_{23} tricyclic terpane over C_{30} hopane; C24Tet/C26T: C_{24} tetracyclic over C_{26} tricyclic terpanes; Gamma/C30H: gammacerane over C_{30} hopane; DBT/Phen: dibenzothiophene over phenanthrene; C18 TAI/AB: ratio of C_{18} trimethyl aryl isoprenoids over C_{18} alkyl benzene; C_{18}: concentration of C_{18} trimethyl aryl isoprenoids in μg/g of extract; C_{13}-C_{22} and C_{15}-C_{31}: concentrations in μg/g of total organic carbon.

Triple Quad MS system in selected ion monitoring (SIM) mode. Split injection (1:10) was employed into a HP-5MS 30 m × 0.25 mm × 0.25 μm capillary column with helium as carrier gas at a flow rate of 1.2 mL/min. Mass spectrometer ion source was operated at 70 eV ionization voltage.

GC–MS analysis of the aromatic fractions was performed on an Agilent 6890 series GC coupled to a 5973 series Mass Selective Detector operated in SIM mode. Split injection was employed into a J&W DB-5 30 m × 0.32 mm × 0.25 μm capillary column at 300 °C temperature. Helium was used as carrier gas at a flow rate of 1.2 mL/min. The GC oven temperature was programmed as follows: 40 °C (at 4 °C/min) → 325 °C (15 min).

Compound identification was based on comparison of GC retention times and mass spectra with those reported in literature and historical data in the GSC-Calgary organic geochemistry laboratories. Appropriate volumes of mixture solutions of internal standards including naphthalene-d8, pHenanthrene-d10 and 1,1-binapthyl were added to the aromatic fractions and C_{29} cholestane-d4 added to the saturated fractions before GC–MS for quantification purposes.

3.4. Other analyses

Also discussed herewith are the ICP (induced coupled-plasma) elemental geochemistry and Rock-Eval pyrolysis results. These data and their acquisition protocols were recently published (Jiang et al., 2016; Kabanov and Gouwy, 2017; Kabanov, 2019), which spares this paper from repetition. The ICP analyses were done for major and trace elements, supplemented by LECO combustion data for total sulfur and carbon. The Rock-Eval 6 pyrolysis-combustion analysis was used to generate total organic carbon (TOC), oxygen index (OI), and hydrogen index (HI) proxies discussed in this paper. Also mentioned are ED-XRF elemental logs from the Kugaluk N-02 well. This technique is amply discussed by Kabanov et al. (2020).

The gamma spectrometry as applied to HRG strata is reviewed in preceding publications (Kabanov et al., 2016b, 2019; Kabanov, 2019). Three spectral gamma proxies found most useful in redox chemostratigraphy (Figs. 3 and 4) are calculated from the U, Th, and K concentrations:

$$SGR[API] = 4 * Th[ppm] + 8 * U[ppm] + 16 * K[wt\%] \quad (1)$$

$$KTH[API] = 4 * Th[ppm] + 16 * K[wt\%] \quad (2)$$

$$U_n = 0.29 * U[ppm] * K[wt\%]^{-1} \quad (3)$$

The concentrations of U, Th, and K are in turn automatically computed in the instrument from spectral series of natural gamma radiation (Ellis and Singer, 2007). Empirical formulas (1) and (2) are widely used as an approximation to total gamma response in API units and its U-stripped component, respectively (*e.g.,* Ellis and Singer, 2007). KTH, also sometimes mnemonized as CGR (computed gamma-ray), is a popular proxy to siliciclastic input (Ellis and Singer, 2007). U_n is mimicking U^*Al^{-1}, the proxy for authigenic U enrichment (*e.g.,* Tribovillard et al., 2006). Substitution of Al with K was made based on strong linear covariation of Al and K observed on 1756 ICP elemental data from the shaly units of the HRG and the basal Imperial Formation (Kabanov, 2019). The slope of 0.29 in formula (3) is a regional signature specific for the siliciclastic provenance.

4. Redox stratigraphy of the horn river group

4.1. Elemental geochemistry and horizons of enhanced anoxia

At least four horizons of enhanced anoxia (AHs) were revealed in the HRG in Little Bear N-09 and Loon Creek O-06 sections based on Al-normalized Mo and U logs from ICP elemental data (Kabanov, 2019), as these trace metals are widely used in elemental proxies interpreting

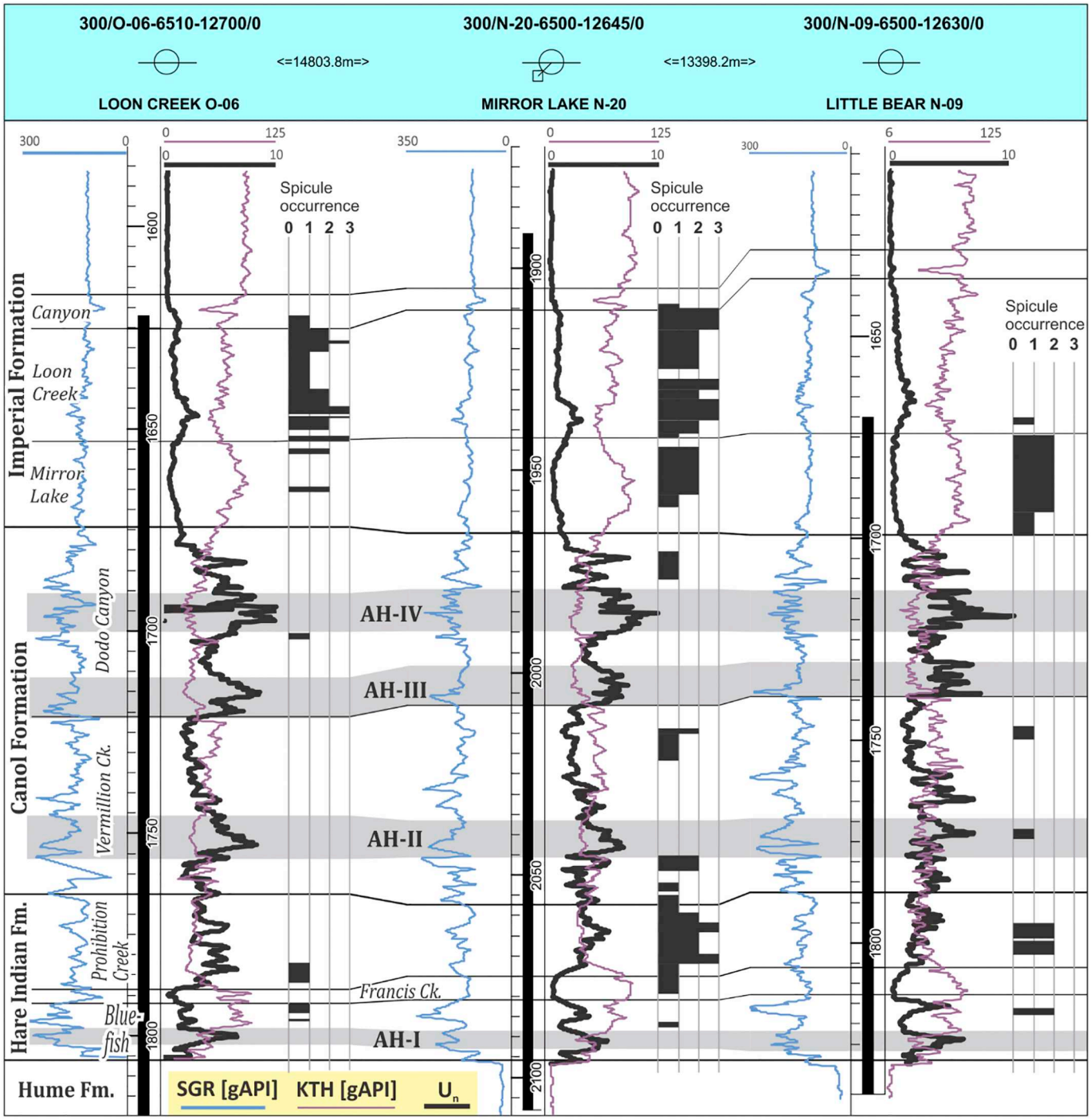

Fig. 4. Occurrence of hyalosponge spicules plotted against spectral gamma-ray proxies in three wells of central Mackenzie Valley (Fig. 2B). Black bars denote core coverage in each well. Occurrence of sponge spicules: (0) no spicules; (1) rare spicules; (2) common spicules – singular spicules are commonly encountered, a few bedding planes may contain spicule meshes; (3) abundant spicules – common spicule meshes on bedding planes.

anoxic sediments (Tribovillard et al., 2006). The revealed AHs, except for AH-I in the HRG base, are characterized by attenuated siliciclastic components as attested by major oxides Al_2O_3, K_2O, TiO_2, and Fe_2O_3 that are known to dominantly reside in siliciclastic detritus (Kabanov, 2019). AHs are partly or completely coincide with horizons of the highest organic-matter richness expressed in TOC (Fig. 3). Very low OI on these horizons (Fig. 3) indicates overwhelmingly planktonogenic origin of kerogen.

The Prohibition Creek Member also exhibits high levels of Al-normalized Mo in Loon Creek O-06 and Little Bear N-09 wells. This enrichment is peering with, and partly exceeding, molybdenum levels at main anoxic horizons (Kabanov, 2019). However, U proxies from ICP and gamma spectrometry do not show equally pronounced enrichment at this interval, and most of wells with available spectralogs do not show U enrichment at all, suspending its interpretation as yet another AH (Kabanov, 2019).

The gamma spectrometry proxies are in excellent agreement with ICP elemental logs from Little Bear N-09 and Loon Creek O-06 wells (Kabanov, 2019). KTH and U_n allow to trace AHs where elemental geochemistry data are not available, particularly in recently drilled exploration wells and the adjacent outcrops of Norman Range within SOB and across the facies zonation in the Rumbly Creek outcrop of the

WOB (Kabanov, 2019). The AHs persist in the fondoformic strata over hundreds of kilometers, as indicated by ED-XRF elemental logs from the continuously cored well Kugaluk N-02 located in ~400 km northward of SOB (Kabanov et al., 2020). AH-III and AH-IV cannot be separated in the thin Canol Formation of the BAT facies zone, and available data do not permit recognition of AH-II there although speculation is made that AH-II may trace as the Carcajou Member of the Ramparts Formation (Fig. 2C; Kabanov, in press).

4.2. Carbon isotope chemostratigraphy

The $\delta^{13}C_{org}$ data from the HRG range from −31.5 to −26.4‰ in their 0.95 percentile bin (Fig. 3), which is perfectly within the range of other Middle-Late Devonian black-shale basins (Van Hengstum and Gröcke, 2008; Meyers, 2014), as well as Triassic and Jurassic black shales based on the compilation of Meyers (2014). The geographically nearest $\delta^{13}C_{org}$ data available from the HRG equivalent black-shale strata show the same range (Fraser and Hutchison, 2017). For the discussion purpose, the organic matter is considered enriched in ^{13}C if $\delta^{13}C_{org}$ crosses the HRG median of −29.07‰ to the right field with higher values (Fig. 3).

The most pronounced positive $\delta^{13}C_{org}$ excursions are labelled with capital letters on Fig. 3: (*A*) in the upper Bluefish-Francis Creek (~ − 28.0‰); (*B*) in the base or just below the AH-II (−27.8‰, max. -27.27‰ in Little Bear N-09); (*C*) in the middle of Mirror Lake member (about −27.1‰, max. -26.4‰); and (*D*) in the Imperial shale in and above the Canyon Member (−27.0‰ to −26.4‰). Positive $\delta^{13}C_{org}$ excursions *A* and *C* correlate with spikes of OI, which in these rocks is a signature of vitrinite enrichment or Type-III organic matter (Fig. 3). Although pyrolysis data are not available above the Loon Creek Member, contribution of coaly particles to the shift *D* is of little doubt as attested on Fig. 3 by high KTH and core observations revealing coaly detritus and dominance of siliciclastic fines in shale composition (Kabanov and Borrero Gomez, 2019).

The $\delta^{13}C_{org}$ excursion *B* does not associate with spikes of terrigenous material and appears to be related to AH-II or, more precisely, to its prelude preceding, and overlapping with, the main phase of U and Mo drawdown from the water column into the sediment (dotted line on Fig. 3). The siliciclastics-lean mudrocks between AHs mostly occur at $\delta^{13}C_{org}$ values ≤29.9‰. This negative background accentuates AH-III and AH-IV as having modest yet distinct ^{13}C enrichments crossing the HRG median (Fig. 3). The lower-middle Bluefish Member containing AH-I exhibits broad spread of data in −30.1‰ to −27.9‰ range with the regression values literally at the HRG median (Fig. 3).

5. Sponge spicules in the horn river group

Hand-lens observations of bedding/fissility planes reveal presence of hyalosponge spicules in cores (Kabanov et al., 2016b; Kabanov and Borrero Gomez, 2019) and outcrops (Kabanov et al., 2019). In dark laminated mudrocks and cherts of the HRG and in similar facies of the basal Imperial Formation, spicules are notably small in size and completely replaced by pyrite (Fig. 5 and Supplementary Appendix 2). No other benthic shelly fossils or metazoan-produced ichnofossils were encountered in anoxic laminated facies. Shales and siltstones of the basal Imperial Formation show overall less severe textural and geochemical signatures of oxygen deficiency (Kabanov and Gouwy, 2017; Kabanov, 2019). Correspondingly, hyalosponge spicules occur in the basal Imperial in plenty (Fig. 4), and many of them, especially larger ones, avoided pyritization (Fig. 5B). SEM examination indicates mimical character of pyrite replacement with perfectly preserved spicule structure (Supplementary Appendix 2). Pyrite replacement of hyalosponge spicules is also known from other world localities of Devonian black shales (*e.g.*, Vishnevskaya et al., 2002).

It should be noted that discontinuous occurrence of sponge spicules in cores (Fig. 4) is a function of taphonomy to much greater extent than real presence-absence. Hard monolithic cores of siliceous mudrocks and cherts of the Canol Formation split along stylolitized bedding planes where no subtle structures such as sponge spicules are preserved. Stylolitization results in similar removal of subtle bedding-plane structures in hard calcareous mudrocks which are abundant in the Hare Indian Formation.

6. Organic geochemistry results

Table 2 presents key biomarker parameters indicative of organic inputs, depositional environments and thermal maturity for shale samples. With their C_{32} hopane 22S/(22S + 22R) ratio being around 0.58–0.62, the Devonian shale intervals from both wells have entered oil generation window, with East Mackay I-78 well being at slightly higher maturity than the Mackenzie River E-27 based on their C_{29} ααα steranes 20S/(20S + 20R) ratios (Table 2). All these black shale samples have a pristane over phytane ratio (Pr/Ph) in the range of 1–2 and a dibenzothiophene over phenanthrene ratio (DBT/Phen) <1, which is consistent with their marine shale lithology (Hughes et al., 1995).

Fig. 6 shows the distributions of 2,3,6- and 3,4,5-trimethl aryl isoprenoids relative to the non-source-specific alkyl benzenes in representative samples. All of the studied shale samples contain high abundances of these aryl isoprenoids ranging from C_{13} to C_{31} as well as a low but recognizable presence of their precursors C_{40} isorenieratanes. The aryl isoprenoids are at much higher abundances than the alkyl benzenes of same carbon numbers (Fig. 6), a distribution pattern that has been reported in the Upper Devonian Bakken shales but not in the overlying Mississippian Lodgepole carbonates from the Williston Basin (Jiang et al., 2001; Aderoju and Bend, 2018). The ratio of C_{18} trimethyl aryl isoprenoids over alkyl benzene (C_{18} TAI/AB) is in the range of 12.41–82.52 for Canol samples and 8.95–11.00 for the Bluefish samples (Table 2), similar to that of the Upper Devonian Bakken shales (9.81–73.46; Jiang et al., 2001). The concentrations of various aryl isoprenoids in the studied HRG samples (Table 2) are higher than those reported for the Bakken shales from Williston Basin (Jiang et al., 2001), the Woodford shales in Arkoma Basin (Connock et al., 2018), and the Famennian Hangenberg black shales from the Polish part of the Laurussian Shelf (Marynowski et al., 2012). For example, the concentration of C_{18} TAI in the solvent extract is up to 1267 μg/g in the Canol samples and as high as 863 μg/g in the Bluefish samples of this study but less than 180 μg/g in the Bakken shales studied by Jiang et al. (2001). The total concentrations of C_{13}-C_{22} TAI relative to the TOC is in the range of 130–578 μg/g TOC in Devonian shales of this study, much higher than that in the Hangenberg black shales from Poland (4.81–13.45 μg/g TOC; Marynowski et al., 2012).

The Canol and Bluefish subsets of samples also show interesting differences in their distributions of tri-, tetra- and penta-cyclic terpanes (Table 2). The Bluefish samples have a C_{23} tricyclic terpane over C_{30} hopane (C23T/C30H) ratio between 2.83 and 3.25, which is much higher than that of the Canol samples where it is mostly below 1 (Table 2). The Bluefish samples also have much higher C_{27} 18α-trisnorneohopane over 17α-trisnorhopane (Ts/Tm) and gammacerane over hopane (Gamma/C30H) ratios than samples from the Canol Formation, all indicating the varying depositional environments and diagenetic conditions. Nevertheless, samples from these two lithostratigraphic units display similar sterane distributions of $C_{27} \approx C_{29} > C_{28}$ (Table 2) which is similar to those reported for the Middle to Upper Devonian black shales of other basins (Creaney and Allan, 1992; Jiang et al., 2001; Connock et al., 2018).

7. Discussion

7.1. Devonian anoxic events in the Horn River Group

Conodont age brackets available to date (data of S.A. Gouwy reviewed by Kabanov, 2019; Gouwy, in press) place the AH-I close to the

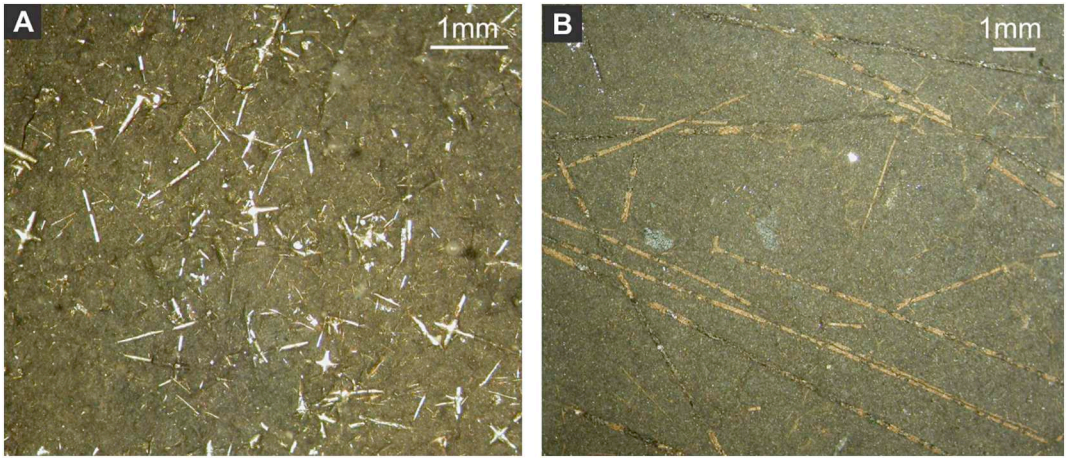

Fig. 5. Hyalosponge spicules under binocular, basal Imperial shales in Mirror Lake N-20 well: (A) smaller spicules replaced by pyrite; (D) larger, non-replaced spicules. More information is given in Supplementary Appendix 2.

Eifelian/Givetian boundary and the global Kačák Event (Fig. 1). The AH-II finds correspondence in the Frasnes event of the basal Frasnian, and AH-II and AH-IV are bundled within the Middle Frasnian, the time of remarkable spread of anoxic sedimentation over continental shelves resulted in the deposition of major hydrocarbon source rocks (Fig. 1; Kabanov, 2019). The AH-III appears to be the expression of the punctata $\delta^{13}C$ excursion of Europe and the Middlesex black shale of the Appalachian foreland basin (Fig. 1; Yans et al., 2007; Pisarzowska and Racki, 2012). The AH-IV in this correlation may be an equivalent of the Rhinestreet black shale of the Appalachians (Fig. 1), although the conodont biostratigraphic identifications are scarce for the upper Canol Formation (Gouwy, in press) leaving a room for further change in age assignments.

The Devonian anoxic events are associated with high-amplitude excursions in $\delta^{13}C$, which in skeletal-carbonate expression are most pronounced at the latest Eifelian – earliest Famennian interval (Fig. 1; Buggisch and Joachimski, 2006; Becker et al., 2012; Saltzman and Thomas, 2012). Fraser and Hutchison (2017) proposed correlation of their $\delta^{13}C_{org}$ positive excursions in the Canol Formation with the $\delta^{13}C_{carb}$ reference curve from GTS-2012 (Fig. 1), which merits extra caution because of totally different carbon fractionation pathways during sedimentation and diagenesis (*e.g.,* Oehlert et al., 2019), and there are examples where $\delta^{13}C_{carb}$ and $\delta^{13}C_{org}$ trends across event horizons are unpaired or even opposite (Cramer and Saltzman, 2007; Oehlert et al., 2019). Available records from the Devonian suggest that anoxic events are expressed as overall positive excursions in both proxies, although not necessarily in significant covariation (Buggisch and Mann, 2004; Van Hengstum and Gröcke, 2008; Śliwiński et al., 2011; Pisarzowska and Racki, 2012; Lash, 2019).

In the HRG, the positive $\delta^{13}C_{org}$ excursions of AH-II, AH-III, and AH-IV (Fig. 3) are overall co-trending with the coeval positive shifts of $\delta^{13}C_{carb}$ in different basins of the World (Fig. 1; Buggisch and Joachimski, 2006; Yans et al., 2007; Śliwiński et al., 2011; Pisarzowska and Racki, 2012; Lash, 2019; Zhang et al., 2019). The AH-I exhibits only minimal positive shift of the regression line and broad spread of data in −30.1‰ to −27.17‰, which may reflect inadequately rare (0.6–0.7 m) sampling in a condensed section masking geologically rapid bidirectional (negative and positive) swings reported from the Kačák interval (Van Hengstum and Gröcke, 2008). Although available $\delta^{13}C_{org}$ data from the AH-I may not look conclusive for establishing the Kačák isotopic shift, other signatures such as abrupt in lithological expression, basinwide switch from the oxic carbonate platform to condensed anoxic sedimentation (Kabanov and Gouwy, 2017; Kabanov, in press) attest for a major redox event at the base of the HRG. Further analysis of the carbon isotope expression of AHs is beyond our scope for this paper. It is sufficient to conclude that new $\delta^{13}C_{org}$ data increase confidence that, within available age constraints, AHs of the HRG are the global Devonian anoxic events.

7.2. Photic-zone euxinia

Aryl isoprenoids with 2,3,6-trimethyl substitution pattern and isorenieratanes are derivatives from isorenieratene, the aromatic carotenoid specific to green sulfur bacteria (GSB) of the family Chlorobiaceae (Koopmans et al., 1996; Imhoff and Thiel, 2010). Obligatory anaerobic phototrophic metabolism of GSB (Imhoff and Thiel, 2010) makes aryl isoprenoids and isorenieratane indicators of PZE (Table 1; Summons and Powell, 1987; Koopmans et al., 1996). Presence of the aryl isoprenoids in all studied samples (Fig. 6 and Table 2) indicates that PZE was a regularly occurring condition. Higher abundance of aryl isoprenoids in Canol samples relative to the Bluefish subset suggests that chemocline was overall shallower during Frasnian or resided in the photic zone for longer periods than during the onset of anoxic sedimentation across the Eifelian/Givetian boundary (Fig. 1C). Higher abundance of aryl isoprenoids in Canol samples might also reflect deeper light penetration in cleaner water as the Canol contains overall less siliciclastic fines than the Bluefish (Figs. 3 and 4; Kabanov and Gouwy, 2017).

7.3. Evidence for fluctuating redox regime

Several lines of evidence attest for the unstable chemocline in the water column, which is not surprising considering how many Devonian-Mississippian black shale basins exhibit signatures of fluctuating redox conditions (*e.g.,* Marynowski et al., 2011, 2012; Martinez et al., 2019). First, the unstable presence of gammacerane and the variation of Gamma/C30H in HRG samples (Table 2) indicates a lack of permanent water-column stratification (Sinninghe Damste et al., 1995). Similar features were reported from other prominent examples of Middle Paleozoic black shales deposited in open-shelf settings (*e.g.*, Marynowski and Filipiak, 2007; Philp and DeGarmo, 2020). The degree of the water column stratification must have varied over the protracted (~388–378 My) HRG deposition, as suggested by higher Gamma/C30H ratio and lower relative abundances of aryl isoprenoids in three Bluefish samples compared to the Canol subset, but the sequence of water stratification events cannot be accurately assessed with the limited number of available biomarker data and the averaged character of samples for biomarkers incorporating dozens of individual sedimentary laminae.

Hyaline sponge spicules provide the other evidence. They are common fossils in suboxic to anoxic fine-grained sediments of the

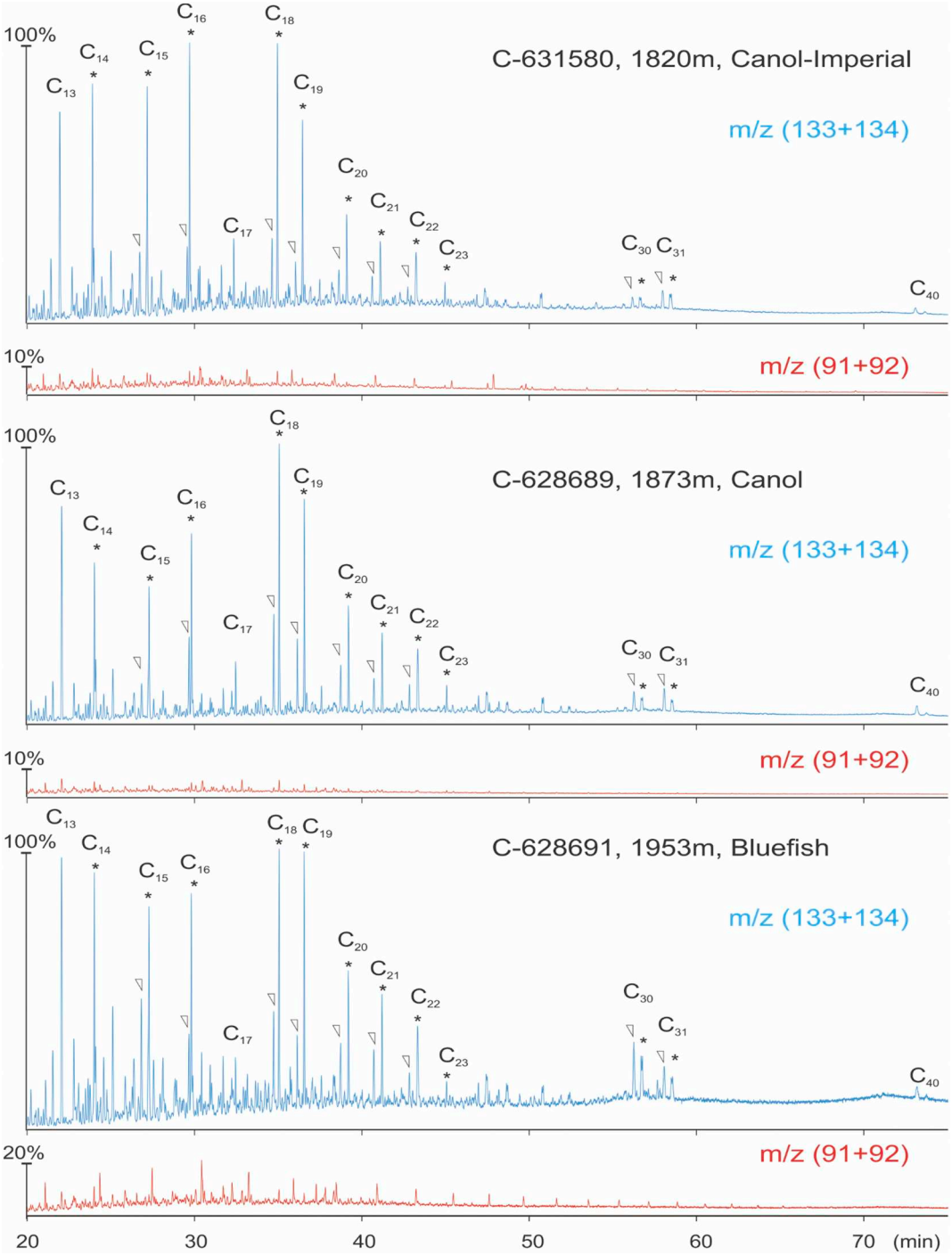

Fig. 6. Mass chromatograms *m/z* (133 + 134) and (91 + 92) showing the distributions of trimethyl aryl isoprenoids and alkyl benzenes in samples from East Mackay I-78. Aryl isoprenoids are significantly more abundant than alkyl benzenes. Peaks labelled by asterisks represent 2,3,6-trimethyl aryl isoprenoids, and those labelled by triangle express 3,4,5-trimethyl aryl isoprenoids.

Phanerozoic where they represent the last evidence of benthic aerobic life in the facies succession towards seafloor euxinia (Racki et al., 2002; Bond and Wignall, 2005; Reolid, 2014). This tolerance to hypoxia originates from the lack of HIF (hypoxia-inducible transcription factors) metabolic pathway in poriferans, whereas in crown-group metazoans HIF maintains stable levels of oxygen in intracellular reactions and shuts down metabolism at certain levels of oxygen starvation (Loenarz et al., 2011; Mills et al., 2018). Sponges survive at oxygen concentrations as low as ~3–8 μM in Peruvian-coast OMZ and in other non-sulphidic anoxic settings where they can endure months of seasonal anoxia (Bell and Barnes, 2000; Levin, 2003; Mosch et al., 2012; Mills et al., 2018). However, an oxygen level of at least 0.5–4% of present-day level seems to be necessary to avoid sponge necrosis, and smaller individuals showed the ability to adapt to the lowest survivable oxygen levels (Mills et al., 2014).

With regards to sponges from the HRG (Fig. 4), the above considerations suggest that the overall anoxic regime would have to be punctuated by periods, probably seasonal, of weak seafloor oxygenation that permitted growth of smaller sponges which were likely represented by different taxonomic groups based on different spicule morphology (Fig. 5 and Supplementary Appendix 2). Mimic substitution of spicules by pyrite (Supplementary Appendix 2) would require rapid micro-

replacement process without creation of an intermediate mold after readily dissolvable opal material (Pisera, 2006; Reolid, 2014). This replacement probably happened during necrosis of a choking sponge at the switch to sulphate reduction inside the sponge body and probably in the ambient water driven into euxinia by the next chemocline rise.

Finally, Mo and U show strong linear covariation ($r^2 \approx 0.7–08$) in black shale units based on representative ($n = 1687$) data from the HRG and the basal Imperial shales (Kabanov, 2019). These black shales are also remarkably enriched in Mo (3–4 times relative to Mo/U ratio in present-day seawater), which is a signature of an oceanographically open anoxic basin with unimpeded resupply of dissolved U and Mo (Kabanov, 2019). This Mo/U signature is very similar to the Cariaco Basin of the southern Caribbean but different from present-day zones of tropical east-coast upwelling and the permanently stratified landlocked basins such as Black Sea (Algeo and Tribovillard, 2009; Tribovillard et al., 2012). In Cariaco Basin, a low sill allows for rapid water renewal with a complete turnover every 50–100 years, and bottom redox conditions frequently fluctuate maintaining the Mn- and Fe-oxyhydroxide shuttling of trace metals as a main factor of covariant Mo and U enrichment in the sediment (Tribovillard et al., 2012; Scholz et al., 2017).

7.4. How deep was the Horn River Group seaway?

Similarity of Mo/U signatures, however, does not make the deep (~1400 m) Cariaco Depression an analog for the HRG sedimentary system. In the latter, the water depth can be estimated based on three assumptions: (1) the HRG accumulated in tectonically quiet setting (Fallas et al., in press; Kabanov, in press) precluding local-scale differential subsidence; (2) the burial compaction caused similar thickness reduction in Hare Indian-Ramparts banks and in the siliceous shales and cherts of adjoining fondoforms; and (3) Kee Scarp banks kept aggrading close to sea level as indicated by the tidal-flat laminites formed in inner bank lagoons of these banks (Yose et al., 2001). In BAT area where carbonate banks are the tallest and likely survived through the entire Canol time, the Hare Indian–Ramparts is *ca.* 350 m (Kabanov and Deblonde, 2019), which approximates the net accommodation space created during HRG deposition. The thickness of Hare Indian and Canol mudrocks deposited in SOB and WOB areas in proximity to BAT shoals is close to 130 m (Kabanov and Deblonde, 2019), which gives a rough estimate of 220 m of net unfilled space in fondoformic seafloor before correction to the lithostatic compaction. As decompaction models are not yet available for the HRG, we can only speculate that the unfilled accommodation space would be restored as approximating 250–300 m by the end of Canol sedimentation.

8. Reduced water energy in an open-shelf basin

Maintenance of water-column stratification with PZE implies shallow storm wave base, which lines up with absence of high-energy facies in the HRG except for its base and the Ramparts Formation. In the HRG base, the evidence for high-energy events is provided by surfaces of storm scouring and thin (≤ 20 cm) brachiopod coquinas with broken, imbricated shells. These coquinas mark the Hume/Bluefish contact (Kabanov and Gouwy, 2017). Graded bioclastic beds can be also encountered in the Ramparts platform member and the Bell Creek Member. Rounded grainstones occur in Kee Scarp banks along with bioturbated packstones. The Kee Scarp banks, although they are frequently called reefs based on plethora of large bulbous stromatoporoids, *Amphipora*, and favositid corals *Thamnopora* (Pugh, 1983; Gal et al., 2009; Pyle and Gal, 2016), show the extreme scarcity of thick marine cements. The latter may be represented by isopachous rims lining intergranular pore space or thicker botryoidal deposits of acicular or radiaxial crystal habits. Radiaxial calcite cements (and very similar fascicular-optic cements) profusely occur in a variety of Paleozoic and Mesozoic carbonate buildups, including mud mounds, and clearly are not restricted to shallow-water marine environments (Flügel, 2010; Richter et al., 2011). However, acicular isopachous rims and botryoids of originally aragonitic composition characterize reef and shoal environments where warm, saturated with Ca^{2+} and Mg^{2+} seawater is continuously pumped through the sediment pore space (review in Flügel, 2010). Furthermore, the best studied oil-producing carbonate bank at Norman Wells lacks facies along its inferred windward margin that would be ascribed to the high-energy reef crest (Yose et al., 2001). In their confirmed occurrences, allochthonous limestones aproning Kee Scarp banks are mostly fine-grained calcarenites and calcisiltiteMackenzie, 1973s with surprisingly few and small (< 5 cm) pebbles and no coarse rubble of corals and stromatoporoids (; Pugh, 1993). This evidence of reduced water energy is not unique to the Kee Scarp but widely reported from Middle Paleozoic carbonate buildups, where controversy in finding reliable water depth indicators allows room for broad interpretations (Hebbeln and Samankassou, 2015).

These signatures of reduced surface-water energy have no explanation by physiographic protection as no evidence for an offshore physiographic barrier or syndepositional blocky tectonics exists across the preserved expanse of the HRG basin (Fallas et al., in press; Kabanov, in press). On broader scale, Laurentian siliciclastic components in the Hare Indian Formation clearly attenuate westward of the BAT zone (Kabanov, 2019), and the Trail River Section at the Peel Shelf – Richardson Trough transition (Fig. 2) is the most depleted in siliciclastics while showing the highest enrichment in authigenic Mo (Fraser and Hutchison, 2017; Kabanov, 2019). In the Selwyn Basin (Fig. 2A), sediments coeval or partly coeval with the HRG are black basinal shales and cherts with submarine hydrothermal metalliferous deposits historically interpreted as SEDEX deposits related to the early phase of ocean-opening rifting (Goodfellow et al., 1993; Magnall et al., 2018). Intervening clastic wedges in the Devonian basinal sequences of the Selwyns are the locally derived lithic conglomerates and sandstones with no evidence of remote sourcing (Gordey and Anderson, 1993; Gordey, 2013). As summarized earlier (Kabanov, 2019), the structural complexity of the Selwyn Basin and controversies in the ANA continental-margin history during the Eifelian-Frasnian time do not allow many conclusive interpretations, but the absence of the barrier between the Peel Shelf sea and Panthalassa appears certain.

8.1. Can Devonian anoxic events be linked to sea level highstands?

In the HRG, the evidence for sea-level fluctuations is only available in Kee Scarp bank-top sections where microbial fenestral laminites, considered the shallowest-water facies, intervene in bioturbated subtidal facies with stromatoporoids and corals (Muir et al., 1984; Yose et al., 2001; Kabanov, 2017; Kabanov and Borrero Gomez, 2019). No obvious subaerial discontinuities are detected in the Kee Scarp.

Although facies repetitions manifesting 4th order cyclicity (0.1–0.5 My; Haq and Shutter, 2008) are not uncommon in coeval shallow-marine strata (Elrick, 1995; Brett and Baird, 1996; Vierek, 2014; Haq and Shutter, 2008; Brady and Bowie, 2017), the evidence of base-level changes is suspiciously short. This is equally true for the 3rd order cycles (0.5–3.0 My; Haq and Shutter, 2008; Haq, 2014) which describe recurrence of anoxic events during the second half of the Devonian (Johnson et al., 1985). Subaerial exposure surfaces separating the 4th order cycles are documented only in the shallowest-water settings such as upper ramps (Elrick, 1995), epicontinental-sea strata (Witzke and Bunker, 1996; Brady and Bowie, 2017) or marine-fluvial cyclic packages (McClung et al., 2013). The depth of pedogenic penetrations and paleokarsts in tops of these cycles is usually described in centimetres (Elrick, 1995; Brady and Bowie, 2017), whereas deeper penetrating (> 1 m) subaerial exposure profiles are rare (*e.g.,* Chen and Tucker, 2004) and do not appear to align at one stratigraphic level in different basins (Hallam and Wignall, 1999). Moreover, awareness increases that paleokarsts associated previously with “major” eustatic lowstands separating 3rd order cycles of Johnson et al. (1985) actually formed in settings of syndepositional blocky tectonics (*e.g.,* Chow et al.,

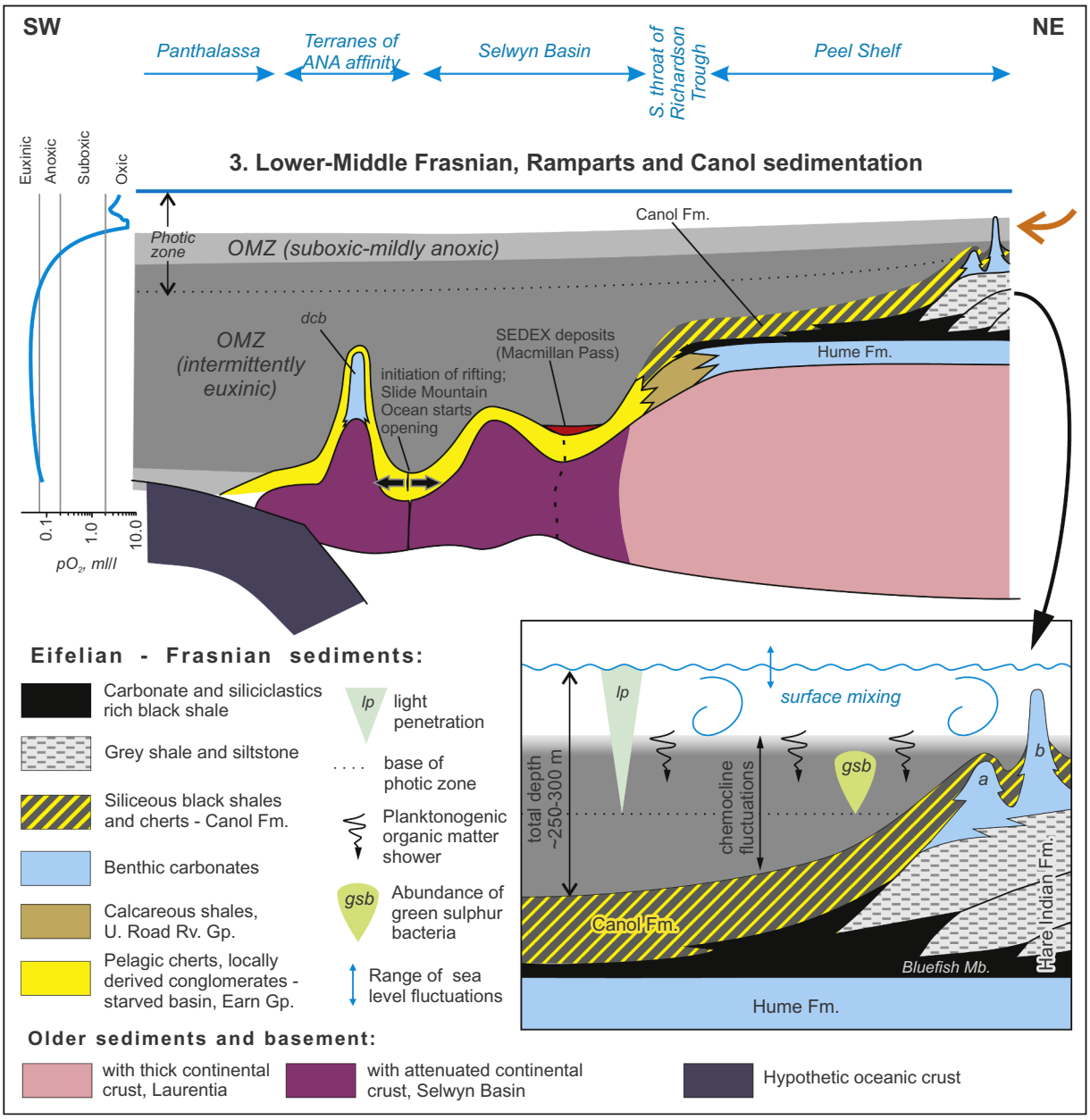

Fig. 7. Hypothetical position of Mackenzie-Peel Shelf in the continental-margin sea of ANA during Middle Frasnian maximum of ocean stratification. The Peel Shelf here is an oceanographically open system impinged by thick oceanic OMZ. Oxygen level on left is based on classification of redox environments (Tyson and Pearson, 1991; Tribovillard et al., 2006). Orange arrow indicates main flux of terrigenous fines from Laurentian sourceland causing hypothetical eastward shallowing of chemocline and light penetration (Kabanov, 2019); *dcb* is drowned Middle Devonian carbonate banks of Fairbanks Terrane (Dusel-Bacon et al., 2006). Geographic extent of this profile is approximated by the torn rectangle on Fig. 2A. **Inset:** more detail of water-column structure; two scenarios for Kee Scarp carbonate banks: (a) smothered by earliest Middle Frasnian rise of anoxic maters (*e.g.,* Norman Wells oil-producing bank); (b) survived Middle Frasnian rise of anoxic maters (centre of BAT zone).

2004).

Another approximation to base level falls are fluvial incisions. Deep (> 10 m) fluvial downcutting is not common in the Middle-Upper Devonian either (Witzke and Bunker, 1996; McClung et al., 2016). Of two cited examples, the deepest incision of 25 m is reported from the area involved in the forebulge of the Appalachian Basin during Acadian compression (McClung et al., 2016). Meagreness of evidence for Devonian sea level fluctuations is particularly lucid in comparison with icehouse sedimentary archives having no shortage of examples of deep, frequent (4th order) base level falls and high-amplitude marine transgressions in the cyclothemic strata (*e.g.,* Soreghan and Giles, 1999; Heckel, 2008; Kabanov et al., 2010; Eriksson et al., 2019).

The above considerations support the visions derating the "major sea-level fluctuations" of the Devonian down to first meters for 4th

order fluctuations and a maximum swing envisioned, still without a conclusive evidence, as ~30 m (*e.g.,* Smith et al., 2019). Possibility that AHs of the HRG do record highstands within this modest sea-level range emerges from their attenuated siliciclastic signatures, which may reflect sourceland retreats in response to sea level rises (Kabanov, 2019). However, the same signature may be equally ascribed to desertification during severing climate differentiation predicted for global warming extremes (Kidder and Worsley, 2010), which is theoretically possible to achieve if sea level is standing still.

Noteworthy, readiness to accept the Devonian anoxic events as sea-level highstands is abated by the conodont $\delta^{18}O$ record from the Upper and Lower Kellwasser events of Paleo-Tethys realm suggesting cooling of surface waters by as much as 6 °C during the Upper Kellwasser (Huang et al., 2018). The $\delta^{18}O$ shifts to heavier values are also recorded in conodont phosphate and carbonate materials at the Early-Middle Frasnian transition and throughout the Middle Frasnian of southern Poland, which translates into a few degrees of water cooling during the maximum spread of anoxic shales (Pisarzowska and Racki, 2012).

Similar debate over the short evidence for sea level fluctuations continues about the Cretaceous warm-greenhouse sedimentary archive, which is much better preserved and relates to the present-day Earth-surface systems more closely than its Devonian counterpart (Sames et al., 2016, 2020; Ray et al., 2020). The main part of the Cretaceous lacks evidence of any form of ice on Earth's surface, but avails cyclic sedimentary successions of 4th to 3rd order indicating sea level fluctuations, which finds support in an array of geochemical proxies. Although the glacio-eustasy is discarded as non-existent or diminutive during the warm-greenhouse and hothouse (Sames et al., 2016, 2020), two hypothetical mechanisms can still be accounted for the 4th and 3rd order sea-level fluctuations. The *thermal eustasy* (a.k.a. *steric sea-level change*) stands for the cyclic expansion-contraction of the oceanic watermass in response to its heating and cooling (Church et al., 2010; Piecuch and Ponte, 2014; Sames et al., 2016). The *aquifer eustasy* refers to the fluctuating proportion of water retained in groundwater reservoirs with minor addition from open waters in lakes and rivers (Wagreich et al., 2014; Sames et al., 2016, 2020; Ray et al., 2020). In the absence of ice, the aquifer water potentially available to cyclically discharge into the ocean and recharge back, is estimated as 8–40 m equivalent of the sea level change (Ray et al., 2020), which is not a conclusive constraint because reliable simulations are not yet available (Sames et al., 2020). The thermal or steric component of the non-glacial eustasy is considered overall minor to the aquifer potential, as not exceeding 10 m on the kyr-scale term, although capable of fast (year-scale) response, which is unavailable for the aquifer eustatic cycles (Sames et al., 2016). Theoretical availability of mechanisms for non-glacial sea level changes, however, does not explain the meagreness of empirical evidence in both the Cretaceous and the Devonian, which casts doubt on sea-level amplitude estimates as routinely exceeding ~25 m in 4th and 3rd order cycles (*e.g.,* Haq and Shutter, 2008; Haq, 2014).

8.2. Towards a consistent oceanographic model

Since sea level control does not withstand scrutiny, the clue to the Devonian pulses of anoxia expressed on continental shelves as synchronous anoxic events is sought in the expansion of oxygen minimum zones into a thick, relatively shallow, and semi-continuous oceanic layer, which is predicted under the warmer greenhouse mode of the Earth (Meyer and Kump, 2008). This scenario of expanded OMZs gains support with arriving data, such as imprints of Kellwasser and Hangenberg anoxias in an oceanic island-arc setting where clearly no room for oceanographic isolation existed (Carmichael et al., 2014, 2016, 2019). Kabanov (2019) discusses this scenario, where thick and shallow OMZ impinges upon the western ANA shelf (Fig. 7) and produces paradoxic (from the actualistic point of view) imprint in the HRG, which spares this paper from repetition. Discovery of PZE biomarkers in the HRG provides solid support for this vision (Fig. 7). No evidence exists on the lateral extension of this OMZ into Panthalassa, as well as the presence or absence of a bottom oxygenated layer, making its depiction on the upper panel of Fig. 7 a speculation awaiting tests with developing knowledge.

Kidder and Worsley (2010) defined the hot, short-living (usually $\leq$1.0 My, rarely up to 3 My) extremes of the greenhouse planetary state as the hothouse condition. The ocean response to hothouse is conceptualized as *haline euxinic acidic thermal transgressions* (HEATT), that are toxic for marine biota and are seen as triggers of mass extinctions (Kidder and Worsley, 2010, 2012; Grasby et al., 2016). The obtained $\delta^{13}C_{org}$ signatures of AHs of the HRG are consistent with global expressions of Devonian anoxic events as overall positive $\delta^{13}C$ excursions (Fig. 1; Bond and Grasby, 2017). However, a fully developed hothouse crisis should show a negative $\delta^{13}C$ swing caused by a drop in primary production as a result of nutrient arrest in expanded OMZs (*e.g.,* Grasby et al., 2016). Fully developed Mesozoic oceanic anoxic events, interpreted as hothouse crises (Hay and Floegel, 2012; Sames et al., 2016, 2020), also record negative excursions of Mo, U and Zn, which are probably a response to drawdown of oceanic inventories of these metals by enhanced precipitation in expanded anoxic waters (Algeo and Rowe, 2012). Such negative swings of trace metals are not observed at peaks of Devonian anoxic events. The lack of evidence for nutrient crises at the majority of Devonian anoxic events led Kidder and Worsley (2010) to interpret these events as nascent HEATTs, and only the Frasnian-Famennian crisis as possibly a fully developed HEATT based on a pilot indication of the negative $\delta^{15}N$ excursion reported by Levman and von Bitter, (2002). The warm-greenhouse to nascent hothouse scenario for the HRG deposition seems to accommodate the evidence for the reduced water energy imprinted in Kee Scarp carbonate buildups as the wind speed is predicted to wane with progressive global warming down to 0.83 of the present-day value in the greenhouse and 0.67 at its extremes in the hothouse, but this calmness might be punctuated by severe cyclonic storms (Kidder and Worsley, 2010).

There are questions still awaiting answers. The evidence for the oceanic nutrient supply in the HRG is controversial and has to reconcile overall oligotrophic characters of the HRG sedimentary system (Kabanov, 2019), and development of massive barite deposits along the eastern margin of Selwyn Basin ascribed to a combination of hydrothermal venting and elevated primary production (Fernandes et al., 2017; Magnall et al., 2018). The expanded OMZs of a warm-greenhouse to hothouse ocean is predicted to effectively remove consumable N, Fe, and micronutrient metals from biochemical cycle while boosting release of bioavailable P (Algeo and Ingall, 2007; Meyer and Kump, 2008; Kidder and Worsley, 2010). In the HRG, phosphorus did not accumulate even in milder anoxic and suboxic facies (Kabanov, 2019) where it would readily precipitate if the sedimentary system were operating through the pathway of a present-day P-rich coastal upwelling zone (Lomnitz et al., 2015). No increase in P content is observed at AHs (Kabanov, 2019), which adds to the inconclusive evidence suggesting overall lean, but occasionally spiking, P_{tot} signatures at Kellwasser anoxic horizons available from the Appalachian Basin and the Paleo-Tethys localities (Percival et al., 2020).

9. Conclusions

The Horn River Group (HRG) of the latest Eifelian – Frasnian Panthalassa-facing continental shelf of Laurentia is an excellent archive of paleoceanographic signals imprinted in oxic and anoxic facies. The HRG basin featured pronounced facies zonation with grey-shale clinoforms and carbonate banks outgrowing these clinoforms. These carbonate banks maintained their growth close to sea level, while laminated black shales and pelagic cherts were deposited in adjacent off-bank (fondoformic) seafloors. These fondoformic sediments deposited at depth estimated as 250–300 m. New biomarker data, occurrence of sponge spicules, strong enrichment in authigenic Mo, and strong Mo/U

covariation indicate that the water-column chemocline was not permanent but remained in fluctuating regime characteristic of an oceanographically open system with unrestricted supply of trace metals from the ocean.

Aryl isoprenoids and isorenieratanes, biomarkers derived from green sulfur reducing bacteria of the family Chlorobiaceae, indicate the frequent and regular reoccurrence of the photic-zone euxinia (PZE) in the redox cycles characterizing the HRG deposition. This finding increases awareness that PZE was a widespread condition in shelfal basins during the second half of the Devonian and early Mississippian (Table 1), the scenario impossible under present-day vigorous thermohaline circulation but consistent with models depicting circulation reversal, drastic slowdown in watermass turnover, and greatly expanded oxygen minimum zones in greenhouse oceans. Biomarker indicators of PZE are also found in the base of the HRG, which is the stratigraphic level of the global Kačák Event (~388 My) where PZE markers are thus reported for the first time.

Horizons of enhanced anoxia (AHs) were revealed in the HRG previously with elemental geochemistry. This work further characterizes AHs with carbon stable isotope data from organic matter ($\delta^{13}C_{org}$) which show positive excursions. These Devonian-Mississippian anoxic events manifest globally as extreme and synchronous spreads of anoxic sediments in shelfal basins, and there are reports of Kellwasser anoxia fingerprinted in oceanic island-arc setting. Although controversial evidence about sea level and cooling-warming histories at the levels of Devonian anoxic events does not permit assertions, data collected in this paper are in favor of interpreting these events as the rises of anoxic waters in response to severing global warming recently defined as a hothouse condition. Lack of indication of nutrient crises at peaks of AHs in our materials supports interpretation of the majority of Devonian anoxic events as nascent, or underdeveloped, hothouse episodes.

The role of sea level rises in anoxic events must have been minor, since no rigorous evidence of sea level fluctuations in excess of several meters is available from the HRG, neither does it seem to be available in the Middle Devonian – Frasnian sedimentary archives of other regions. The most reasonable explanation of attenuated siliciclastic signature of AHs is seen in sourceland retreats in response to non-glacial (thermal and aquifer) eustatic transgressions.

Supplementary data to this article can be found online at https://doi.org/10.1016/j.gloplacha.2020.103153.

Acknowledgements

This work is a contribution to the Geoscience for New Energy Supplies (GNES) Programme, Geological Survey of Canada (Lands and Minerals Sector, Natural Resources Canada) publication No. 20190543. Edward Little and Margaret Ferguson (both GSC Calgary) provided administrative support, and M. Ferguson also performed style editing in the early version. Thorough improvement of the final version was made possible thanks to peer-reviews by three anonymous reviewers and the extensive editorial advice from Grzegorz Racki (U. of Sosnowiec, Poland). Analytical work has been conducted in previous years under GEM Western Arctics Project (stable isotope study) and GEM Mackenzie Project (biomarker study) with critical support from Carl Ozyer and Thomas Hadlari (both GSC Calgary). Gratitude comes to Stephen Grasby (GSC Calgary) for providing the lab for sample preparation (and also remarks through the text) and Mary Luz Borrero Gomez who crushed and decarbonated samples for the carbon isotope study in this lab; to Paul Middlestead, Wendy Abdi, and Patricia Wickham who performed carbon isotope analyses at the G.G. Hatch Laboratory of the University of Ottawa. Sampling for biomarker study was authorized by OROGO with approval SR-2017-003 from 2018/01/10 (East McKay I-78 well) and by NEB with authorization # 12624 from 2016/11/30 (Mackenzie River # 4 well). Sampling for the carbon isotope study was conducted with OROGO approval SR-2017-004. This work is also part of the IGCP-652 Project “Reading geologic time in Palaeozoic sedimentary rocks”.

References

AANDC, 2014. Northern Oils and Gas Annual Report for 2013. 30 p. http://www.aadnc-aandc.gc.ca/eng/1398800136775/1398800252896#chp3 Accessed on 29-02-2020.

Aderoju, T., Bend, S., 2018. Reconstructing the palaeoecosystem and palaeodepositional environment within the Upper Devonian–Lower Mississippian Bakken Formation: a biomarker approach. Org. Geochem. 119, 91–100. https://doi.org/10.1016/j.orggeochem.2018.03.003.

Algeo, T.J., Ingall, E., 2007. Sedimentary C_{org}: P ratios, paleocean ventilation, and Phanerozoic atmospheric pO2. Palaeogeogr. Palaeoclimatol. Palaeoecol. 256, 130–155. https://doi.org/10.1016/j.palaeo.2007.02.029.

Algeo, T.J., Rowe, H., 2012. Paleoceanographic applications of trace-metal concentration data. Chem. Geol. 324–325, 6–18. https://doi.org/10.1016/j.chemgeo.2011.09.002.

Algeo, T.J., Scheckler, S.E., 1998. Terrestrial-marine teleconnections in the Devonian: links between the evolution of land plants, weathering processes, and marine anoxic events. Phil. Trans. R. Soc. B: Biol. Sci. 353, 113–130. https://doi.org/10.1098/rstb.1998.0195.

Algeo, T.J., Tribovillard, N., 2009. Environmental analysis of paleoceanographic systems based on based on molybdenum–uranium covariation. Chem. Geol. 268, 211–225. https://doi.org/10.1016/j.chemgeo.2009.09.001.

Algeo, T.J., Fisk, N.H., Berner, R.A., Maynard, J.B., Scheckler, S.E., 1995. Late Devonian oceanic anoxic events and biotic crises: ‘Rooted’ in the evolution of vascular land plants? GSA Today 5, 64–66.

Arthur, M.A., Sageman, B.B., 2005. Sea-level control on source-rock development: perspectives from the Holocene Black Sea, the mid-Cretaceous Western Interior Basin of North America, and the Late Devonian Appalachian Basin. SEPM Spec. Publ. 82, 35–59. https://doi.org/10.2110/pec.05.82.0035.

Becker, R.T., Gradstein, F.M., Hammer, O., 2012. The Devonian period. In: Gradstein, F.M., Ogg, J.G., Schmitz, M., Ogg, G. (Eds.), The Geologic Time Scale 2012. vol. 2. Elsevier, Amsterdam, pp. 559–601. https://doi.org/10.1016/B978-0-444-59425-9.00022-6.

Becker, R.T., Königshof, P., Brett, C.E., 2016. Devonian climate, sea level and evolutionary events: an introduction. In: Becker, R.T., Königshof, P., Brett, C.E. (Eds.), Devonian Climate, Sea Level and Evolutionary Events. Geological Society, London, Special Publications. 423pp. 1–10. https://doi.org/10.1144/SP423.15.

Bell, J.J., Barnes, D.K.A., 2000. A sponge diversity centre within a marine ‘island’ In: Jones, M.B., Azevedo, J.M.N., Neto, A.I., Costa, A.C., Martins, A.M. Frias (Eds.), Island, Ocean and Deep-Sea Biology, Proceedings of the 34th European Marine Biology Symposium, held in Ponta Delgada (Azores), Portugal, September 13–17, 1999.

Beranek, L.P., Mortensen, J.K., Lane, L., Allen, T., Fraser, T., Hadlari, T., Zantvoort, W.G., 2010. Detrital zircon geochronology of the western Ellesmerian clastic wedge, northwestern Canada: insights on Arctic tectonics and evolution of the northern Cordilleran miogeocline. Geol. Soc. Am. Bull. 122, 1899–1911. https://doi.org/10.1130/B30120.1.

Bond, D.P.G., Grasby, S.E., 2017. On the causes of mass extinctions. Palaeogeogr. Palaeoclimatol. Palaeoecol. 478, 3–29. https://doi.org/10.1016/j.palaeo.2016.11.005.

Bond, D.P.G., Wignall, P.B., 2005. Chapter 9. Evidence for Late Devonian (Kellwasser) anoxic events in the Great Basin, western United States. In: Over, D.J., Morrow, J.R., Wignall, P.B. (Eds.), Understanding Late Devonian and Permian-Triassic Biotic and Climatic Events, Development in Palaeontology and Stratigraphy 20. Elsevier, pp. 225–261. https://doi.org/10.1016/S0920-5446(05)80009-3.

Bond, D.P.G., Wignall, P.B., 2008. The role of sea-level change and marine anoxia in the Frasnian–Famennian (Late Devonian) mass extinction. Palaeogeogr. Palaeoclimatol. Palaeoecol. 263, 107–118. https://doi.org/10.1016/j.palaeo.2008.02.015.

Bond, D.P.G., Wignall, P.B., 2014. Large igneous provinces and mass extinctions: an update. In: Keller, G., Kerr, A.C. (Eds.), Volcanism, Impacts, and Mass Extinctions: Causes and Effects. Geological Society of America Special Paper, 505pp. 29–55. https://doi.org/10.1130/2014.2505(02).

Bond, D.P.G., Wignall, P.B., Racki, G., 2004. Extent and duration of marine anoxia during the Frasnian-Famennian (Late Devonian) mass extinction in Poland, Germany, Austria, and France. Geol. Mag. 141, 173–193. https://doi.org/10.1017/S0016756804008866.

Brady, M., Bowie, C., 2017. Discontinuity surfaces and microfacies in a storm dominated shallow Epeiric Sea, Devonian Cedar Valley Group, Iowa. Depos. Rec. 3, 136–160. https://doi.org/10.1002/dep2.26.

Brett, C.E., Baird, G.C., 1996. Middle Devonian sedimentary cycles and sequences in the northern Appalachian basin. In: Witzke, B.J., Ludvigson, G.A., Day, J. (Eds.), Paleozoic Sequence Stratigraphy: Views from the North American Craton. Geological Society of America Special Paper. 306pp. 213–241.

Brett, C.E., Baird, G.C., Bartholomew, A.J., DeSantis, M.K., Ver Straeten, C.A., 2011. Sequence stratigraphy and a revised sea-level curve for the Middle Devonian of eastern North America. Palaeogeogr. Palaeoclimatol. Palaeoecol. 304, 21–53. https://doi.org/10.1016/j.palaeo.2010.10.009.

Brown, T.C., Kenig, F., 2004. Water column structure during deposition of Middle Devonian–Lower Mississippian black and green/gray shales of the Illinois and Michigan Basins: a biomarker approach. Palaeogeogr. Palaeoclimatol. Palaeoecol. 215, 59–85. https://doi.org/10.1016/j.palaeo.2004.08.004.

Buggisch, W., Joachimski, M.M., 2006. Carbon isotope stratigraphy of the Devonian of Central and Southern Europe. Palaeogeogr. Palaeoclimatol. Palaeoecol. 240, 68–88. https://doi.org/10.1016/j.palaeo.2006.03.046.

Buggisch, W., Mann, U., 2004. Carbon isotope stratigraphy of Lochkovian to Eifelian

limestones from the Devonian of central and southern Europe. Int. J. Earth Sci. (Geol. Rundsch.) 93, 521–541. https://doi.org/10.1007/s00531-004-0407-6.
Bushnev, D.A., Burdel'naya, N.S., Ponomarenko, E.S., Zubova, T.A., 2016. Anoxia in the Domanik basin of the Timan–Pechora region. Lithol. Miner. Resour. 51, 283–289. https://doi.org/10.1134/S0024490216040027.
Carmichael, S.K., Waters, J.A., Suttner, T.J., Kido, E., DeReuil, A.A., 2014. A new model for the Kellwasser anoxia events (Late Devonian): shallow water anoxia in an open oceanic setting in the central Asian Orogenic belt. Palaeogeogr. Palaeoclimatol. Palaeoecol. 399, 394–403. https://doi.org/10.1016/j.palaeo.2014.02.016.
Carmichael, S.K., Waters, J.A., Batchelor, C.J., Coleman, D.M., Suttner, T.J., Kido, E., Moore, L.M., Chadimová, L., 2016. Climate instability and tipping points in the Late Devonian: detection of the Hangenberg event in an open oceanic island arc in the central Asian Orogenic Belt. Gondwana Res. 32, 213–231. https://doi.org/10.1016/j.gr.2015.02.009.
Carmichael, S.K., Waters, J.A., Königshof, P., Suttner, T.J., Kido, E., 2019. Paleogeography and paleoenvironments of the Late Devonian Kellwasser event: a review of its sedimentological and geochemical expression. Glob. Planet. Chang. 183. https://doi.org/10.1016/j.gloplacha.2019.102984.
Chen, D., Tucker, M., 2004. Palaeokarst and its implication for the extinction event at the Frasnian–Famennian boundary (Guilin, South China). J. Geol. Soc. Lond. 161, 895–898. https://doi.org/10.1144/0016-764904-034.
Chow, N., George, A.D., Trinajstic, K.M., 2004. Tectonic control on development of a Frasnian–Famennian (Late Devonian) palaeokarst surface, Canning Basin reef complexes, northwestern Australia. Aust. J. Earth Sci. 51, 911–917. https://doi.org/10.1111/j.1400-0952.2004.01493.x.
Church, J.A., Roemmich, D., Domingues, C.M., Willis, J.K., White, N.J., Gilson, J.E., Stammer, D., Köhl, A., Chambers, D.P., Landerer, F.W., Marotzke, J., Gregory, J.M., Suzuki, T., Cazenave, A., Le Traon, P.-Y., 2010. Chapter 6. Ocean temperature and salinity contributions to global and regional sea-level change. In: Church, J.A., Woodworth, P.L., Aarup, T., Wilson, W.S. (Eds.), Understanding Sea-Level Rise and Variability, 1st ed. Wiley-Blackwell, Chichester, pp. 143–176 ISBN: 978-1-444-33452-4.
Cohen, K.M., Finney, S.C., Gibbard, P.L., Fan, J.-X., 2013. The ICS international chronostratigraphic chart. Episodes 36, 199–204. (updated in 2018). URL: http://www.stratigraphy.org/ICSchart/ChronostratChart2018-08.pdf Accessed March 02, 2020.
Colpron, M., Nelson, J.L., 2011. A digital atlas of Terranes for the Northern Cordillera. B.C. GeoFile 2011–11. https://www2.gov.bc.ca/gov/content/industry/mineral-exploration-mining/british-columbia-geological-survey/publications/geofiles, Accessed date: 4 March 2020.
Connock, G.T., Nguyen, T.X., Philp, R.P., 2018. The development and extent of photic-zone euxinia concomitant with Woodford Shale deposition. AAPG Bull. 102, 959–986. https://doi.org/10.1306/0726171602017224.
Cramer, B.D., Saltzman, M.R., 2007. Early Silurian paired $\delta^{13}C_{carb}$ and $\delta^{13}C_{org}$ analyses from the Midcontinent of North America: implications for paleoceanography and paleoclimate. Palaeogeogr. Palaeoclimatol. Palaeoecol. 256, 195–203. https://doi.org/10.1016/j.palaeo.2007.02.032.
Creaney, S., Allan, J., 1992. Petroleum systems in the Foreland Basin of Western Canada. In: Macqueen, R.W., Leckie, D.A. (Eds.), Foreland Basins and Fold Belts. American Association of Petroleum Geologists Memoir 55pp. 279–309.
Dong, T., Harris, N.B., Ayranci, K., 2018. Relative sea-level cycles and organic matter accumulation in shales of the Middle and Upper Devonian Horn River Group, northeastern British Columbia, Canada: insights into sediment flux, redox conditions, and bioproductivity. Geol. Soc. Am. Bull. 130, 859–880. https://doi.org/10.1130/B31851.1.
Dusel-Bacon, C., Hopkins, M.J., Mortensen, J.K., Dashevsky, S.S., Bressler, J.R., Day, W.C., 2006. Paleozoic tectonic and metallogenic evolution of the pericratonic rocks of east-central Alaska and adjacent Yukon. In: Colpron, M., Nelson, J.L. (Eds.), Paleozoic Evolution and Metallogeny of Pericratonic Terranes at the Ancient Pacific Margin of North America. Canadian and Alaskan Cordillera. Geological Association of Canada Special Paper. 45pp. 25–74.
Ellis, D.V., Singer, J.M., 2007. Well Logging for Earth Scientists, 2nd ed. Springer 692 p. ISBN: 978-1-4020-4602-5.
Elrick, M., 1995. Cyclostratigraphy of Middle Devonian carbonates of the eastern Great Basin. J. Sediment. Res. B65, 61–79. https://doi.org/10.1306/D42681E4-2B26-11D7-8648000102C1865D.
Eriksson, K.A., McClung, W.S., Simpson, E.L., 2019. Sequence stratigraphic expression of greenhouse, transitional and icehouse conditions in siliciclastic successions: Paleozoic examples from the central Appalachian basin, USA. Earth Sci. Rev. 188, 176–189. https://doi.org/10.1016/j.earscirev.2018.11.010.
Ernst, R.E., Rodygin, S.A., Grinev, O.M., 2020. Age correlation of Large Igneous Provinces with Devonian biotic crises. Glob. Planet. Chang. 185. https://doi.org/10.1016/j.gloplacha.2019.103097.
Ettensohn, F.R., 1994. Tectonic control on formation and cyclicity of major Appalachian unconformities and associated stratigraphic sequences. In: Dennison, J.M., Ettensohn, F.R. (Eds.), Tectonic and Eustatic Controls on Sedimentary Cycles. SEPM (Society for Sedimentary Geology) Concepts in Sedimentology and Paleontology. 4pp. 217–242.
Falkowski, P.G., Algeo, T., Codispoti, L., Deutsch, C., Emerson, S., Hales, B., Huey, R.B., Jenkins, W.J., Kump, L.R., Levin, L.A., Lyons, T.W., Nelson, N.B., Schofield, O.S., Summons, R., Talley, L.D., Thomas, E., Whitney, F., Pilcher, C.B., 2011. Ocean deoxygenation: past, present, and future. EOS. 92, 409–420. https://doi.org/10.1029/2011EO460001.
Fallas, K.M., MacNaughton, R.B., 2013. Geology, Norman Wells (Southeast), Northwest Territories; Geological Survey of Canada, Canadian Geoscience Map 100, Scale 1:100,000.
Fallas, K.M., MacNaughton, R.B., 2019. GEM-Mackenzie: bedrock mapping and related stratigraphic studies, 2009–2019. Geol. Surv. Can. https://doi.org/10.4095/314799. Open File 8587. 55 p.
Fallas, K.M., MacNaughton, R.B., Hannigan, P.K., and MacLean, B.C. (in press). Mackenzie-Peel Platform and Ellesmerian Foreland Tectono-Sedimentary Elements, northwestern Canada. In: Moore, T.E, and Drachev, S.S. (eds.), Arctic Tectono-Sedimentary Elements and Their Hydrocarbon Prospectivity. Geological Society of London, Memoir
Fernandes, N.A., Gleeson, S.A., Magnall, J.M., Creaser, R.A., Martel, E., Fischer, B.J., Sharp, R., 2017. The origin of Late Devonian (Frasnian) stratiform and stratabound mudstone-hosted barite in the Selwyn Basin, Northwest Territories, Canada. Mar. Pet. Geol. 85, 1–15. https://doi.org/10.1016/j.marpetgeo.2017.04.006.
Flügel, E., 2010. Microfacies of Carbonate Rocks. Analysis, Interpretation and Application, 2nd ed. Springerhttps://doi.org/10.1007/10.1007/978-3-642-03796-2. 984 p.
Fraser, T.A., Hutchison, M.P., 2017. Lithogeochemical characterization of the Middle–Upper Devonian Road River Group and Canol and Imperial formations on Trail River, east Richardson Mountains, Yukon: age constraints and a depositional model for fine-grained strata in the Lower Paleozoic Richardson trough. Can. J. Earth Sci. 54, 731–765. https://doi.org/10.1139/cjes-2016-0216.
Gabrielse, H., Yorath, C.J., 1991. Chapter 1. Introduction. In: Gabrielse, H., Yorath, C.J. (Eds.), Geology of the Cordilleran orogen in Canada. Geological Survey of Canada, Geology of Canada. 4pp. 3–15. https://doi.org/10.4095/134069.
Gal, L.P., Pyle, L.J., Hadlari, T., Allen, T.L., 2009. Chapter 6 – Lower to Upper Devonian strata, Arnica–Landry Play, and Kee Scarp Play. In: Pyle, L.J., Jones, A.L. (Eds.), Regional Geoscience Studies and Petroleum Potential, Peel Plateau and Plain, Northwest Territories and Yukon. Project Volume, pp. 187–289 NWT Open File 2009-02 and YGS Open File 2009-25.
Gatovskii, Yu.A., Stupakova, A.V., Kalmykov, G.A., Korobova, N.I., Suslova, A.A., Sautkin, R.S., Kalmykov, D.G., 2016. New data on the biostratigraphy and facies types of upper Devonian Domanik sections in the Volga-Ural Basin. Mosc. Univ. Geol. Bull. 71, 58–70. https://doi.org/10.3103/S014587521505004X.
Goodfellow, W.D., Lydon, J.W., Turner, R.J., 1993. Geology and genesis of stratiform sediment-hosted (SEDEX) zinc-lead-silver sulphide deposits. In: Kirkham, R.W., Sinclair, R., Thorpe, R.I., Duke, J.M. (Eds.), Mineral Deposit Modeling. Geological Association of Canadapp. 201–252.
Gordey, S.P., 2013. Evolution of the Selwyn Basin, Sheldon Lake and Tay River map areas, central Yukon. Geol. Surv. Can. Bull. 599. https://doi.org/10.4095/293034.
Gordey, S.P., Anderson, R.G., 1993. Evolution of the northern Cordilleran miogeocline, Nahanni map area (105I), Yukon and Northwest Territories. Geol. Surv. Can. Mem. 428. https://doi.org/10.4095/183983.
Gouwy, S.A. (In press). Devonian conodont biostratigraphy of the Mackenzie Mountains (NWT, Canada). In: Lavoie, D. and Dewing, K. (eds.), Sedimentary basins of the Canadian north - Contributions to a 1000 Ma geological journey and insight on resource potential; Geological Survey of Canada Bulletin 609, paper 6
Grasby, S.E., Beauchamp, B., Knies, J., 2016. Early Triassic productivity crises delayed recovery from world's worst mass extinction. Geology. 44, 779–782. https://doi.org/10.1130/G38141.1.
Haddad, E.E., Tuite, M.L., Martinez, A.M., Willford, K., Boyer, D.L., Droser, M.L., Love, G.D., 2016. Lipid biomarker stratigraphic records through the Late Devonian Frasnian/Famennian boundary: comparison of high- and low-latitude epicontinental marine settings. Org. Geochem. 98, 38–53. https://doi.org/10.1016/j.orggeochem.2016.05.007.
Hadlari, T., Tylosky, S.A., Lemieux, Y., Zantvoort, W.G., Catuneanu, O., 2009. Slope and submarine fan turbidite facies of the Upper Devonian Imperial Formation, northern Mackenzie Mountains, NWT. Bull. Can. Petrol. Geol. 57, 192–208. https://doi.org/10.2113/gscpgbull.57.2.192.
Hallam, A., Wignall, P.B., 1999. Mass extinctions and sea-level changes. Earth Sci. Rev. 48, 217–250. https://doi.org/10.1016/S0012-8252(99)00055-0.
Haq, B.U., 2014. Cretaceous eustasy revisited. Glob. Planet. Chang. 113, 44–58. https://doi.org/10.1016/j.gloplacha.2013.12.007.
Haq, B.U., Shutter, S.R., 2008. A chronology of paleozoic sea-level changes. Science. 322, 64–68. https://doi.org/10.1126/science.1161648.
Hay, W.W., Floegel, S., 2012. New thoughts about the cretaceous climate and oceans. Earth Sci. Rev. 115, 262–272. https://doi.org/10.1016/j.earscirev.2012.09.008.
Hebbeln, D., Samankassou, E., 2015. Where did ancient carbonate mounds grow – in bathyal depths or in shallow shelf waters? Earth Sci. Rev. 145, 56–65. https://doi.org/10.1016/j.earscirev.2015.03.001.
Heckel, P.H., 2008. Pennsylvanian cyclothems in Midcontinent North America as far-field effects of waxing and waning of Gondwana ice sheets. In: Fielding, C.R., Frank, T.D., Isbell, J.L. (Eds.), Resolving the Late Paleozoic Ice Age in Time and Space. Geological Society America, Special Paper 441pp. 275–289. https://doi.org/10.1130/2008.2441(19).
House, M.R., 1983. Devonian eustatic events. Proc. Ussher Soc. 6, 396–405.
House, M.R., 1996. The Middle Devonian Kačák event. Proc. Ussher Soc. 9, 79–84.
House, M.R., 2002. Strength, timing, setting and cause of mid-Palaeozoic extinctions. Palaeogeogr. Palaeoclimatol. Palaeoecol. 181, 5–25. https://doi.org/10.1016/S0031-0182(01)00471-0.
House, M.R., Menner, V.V., Becker, R.T., Klapper, G., Ovnatanova, N.S., Kuzmin, A.V., 2000. Reef episodes, anoxia and sea-level changes in the Frasnian of the southern Timan (NE Russian Platform). In: Insalaco, E., Skelton, P.W., Palmer, T.J. (Eds.), Carbonate Platform Systems: Components and Interactions. Geological Society of London, Special Publications 178. pp. 147–176. https://doi.org/10.1144/GSL.SP.2000.178.01.11.
Huang, C., Joachimski, M.M., Gong, Y., 2018. Did climate changes trigger the Late Devonian Kellwasser Crisis? Evidence from a high-resolution conodont $\delta^{18}O_{PO4}$ record from South China. Earth Planet. Sci. Lett. 495, 174–184. https://doi.org/10.1016/j.epsl.2018.05.016.

Hughes, W.B., Holba, A.G., Dzou, L.I.P., 1995. The ratio of dibenzothiophene to phenanthrene and pristane to phytane as indicators of depositional environment and lithology of petroleum source rocks. Geochim. Cosmochim. Acta 59, 3581–3598. https://doi.org/10.1016/0016-7037(95)00225-O.

Imhoff, J.F., Thiel, V., 2010. Phylogeny and taxonomy of *Chlorobiaceae*. Photosynth. Res. 104, 123–136. https://doi.org/10.1007/s11120-009-9510-7.

Jiang, C., Li, M., Osadetz, K.G., Snowdon, L.R., Obermajer, M., Fowler, M.G., 2001. Bakken/Madison petroleum systems in the Canadian Williston Basin. Part 2: molecular markers diagnostic of Bakken and Lodgepole source rocks. Org. Geochem. 32, 1037–1054. https://doi.org/10.1016/s0146-6380(01)00016-x.

Jewell, P.W., 1994. Paleoredox Conditions and the Origin of Bedded Barites along the Late Devonian North American Continental Margin. J. Geol. 102, 151–164. https://doi.org/10.1086/629660.

Jiang, C., Chen, Z., Mort, A., Milovic, M., Robinson, R., Stewart, R., Lavoie, D., 2016. Hydrocarbon evaporative loss from shale core samples as revealed by Rock-Eval and thermal desorption-gas chromatography analysis: its geochemical and geological implications. Mar. Pet. Geol. 70, 294–303. https://doi.org/10.1016/j.marpetgeo.2015.11.021.

Jiang, C., Obermajer, M., Kabanov, P., Mort, A., 2020. Organic geochemical data from Northern Canada. Part II: Biomarkers in organic extracts from Devonian black shales (Horn River Group and basal Imperial Formation), Norman Wells area, Northwest Territories. Geol. Surv. Can. https://doi.org/10.4095/321479. Open File 8663.

Joachimski, M.M., Ostertag-Henning, C., Pancost, R.D., Strauss, H., Freeman, K.H., Littke, R., Damste, J.S.S., Racki, G., 2001. Water column anoxia, enhanced productivity and concomitant changes in $\delta^{13}C$ and in $\delta^{34}S$ across the Frasnian–Famennian boundary (Kowala Holy Cross Mountains/Poland). Chem. Geol. 175, 109–131. https://doi.org/10.1016/S0009-2541(00)00365-X.

Johnson, J.G., Klapper, G., Sandberg, C.A., 1985. Devonian eustatic fluctuations in Euramerica. Geol. Soc. Am. Bull. 96, 567–587. https://doi.org/10.1130/0016-7606(1985)96<567:DEFIE>2.0.CO;2.

Johnston, D.I., Henderson, C.M., Schmidt, M.J., 2010. Upper Devonian to Lower Mississippian conodont biostratigraphy of uppermost Wabamun Group and Palliser Formation to lowermost Banff and Lodgepole formations, southern Alberta and southeastern British Columbia, Canada: Implications for correlations and sequence stratigraphy. Bull. Can. Petrol. Geol. 58, 295–341. https://doi.org/10.2113/gscpgbull.58.4.295.

Kabanov, P., 2017. Geological and geochemical data from Mackenzie Corridor. Part VII: new geochemical, Rock-Eval 6, and field data from the Ramparts and Canol formations of northern Mackenzie Valley, Northwest Territories. Geol. Surv. Can. https://doi.org/10.4095/306368. Open File, 8341.

Kabanov, P., 2019. Devonian (c. 388-375 my) Horn River Group of Mackenzie Platform (northwestern Canada) is an open-shelf succession recording oceanic anoxic events. J. Geol. Soc. Lond. 176, 29–45. https://doi.org/10.1144/jgs2018-075.

Kabanov, P., (In press). Devonian of the Mackenzie. In: Lavoie, D. and Dewing, K. (Eds.): Sedimentary basins of the Canadian North - Contributions to a 1000 Ma geological journey and insight on resource potential; Geological Survey of Canada, Bulletin 609, paper 7.

Kabanov, P., Borrero Gomez, M.L., 2019. Geological and geochemical data from Mackenzie Corridor. Part IX: descriptions and associated measurements of cores from the Middle and Upper Devonian, Northwest Territories. Geol. Surv. Can. https://doi.org/10.4095/314982. Open File 8558, 162 p.

Kabanov, P., Deblonde, C., 2019. Geological and geochemical data from Mackenzie Corridor. Part VIII: Middle-Upper Devonian lithostratigraphy, formation tops and isopach maps in NTS areas 96 and 106, Northwest Territories and Yukon. Geol. Surv. Can. https://doi.org/10.4095/314785. Open File 8552.

Kabanov, P., Gouwy, S., 2017. The Devonian Horn River Group and the basal Imperial Formation of the Central Mackenzie Plain, N.W.T., Canada: Multiproxy stratigraphic framework of a black shale basin. Can. J. Earth Sci. 54, 409–429. https://doi.org/10.1139/cjes-2016-0096.

Kabanov, P., Alekseeva, T., Alekseev, A., Alekseeva, V., Gubin, S., 2010. Paleosols in Late Moscovian (Carboniferous) marine carbonates of East European Craton revealing "Great Calcimagnesian Plain" paleolandscapes. J. Sediment. Res. 80, 195–215. https://doi.org/10.2110/jsr.2010.026.

Kabanov, P., Fallas, K.M., Deblonde, C., 2016a. Geological and geochemical data from Mackenzie Corridor. Part IV: formation tops and isopach maps of Horn River Group and basal beds of Imperial Formation, Central Mackenzie Plain, NTS map sheets 96C-E. Geol. Surv. Can. Open File 8023. https://doi.org/10.4095/297903.

Kabanov, P., Gouwy, S., Lawrence, P.W., Weleschuk, D.J., Chan, W.C., 2016b. Geological and geochemical data from Mackenzie Corridor. Part III: new data on lithofacies, micropaleontology, lithogeochemistry, and Rock-Eval pyrolysis, Devonian Horn River Group of Mackenzie Plain and Norman Range. Geol. Surv. Can. https://doi.org/10.4095/297832. Open File 7951.

Kabanov, P., VandenBerg, R., Gouwy, S., van der Boon, A., Thallner, D., Biggin, A., 2019. Geological and geochemical data from Mackenzie corridor. Part X: reference sections of Middle-Upper Devonian strata at Prohibition Creek, Norman Range, Northwest Territories. Geol. Surv. Can. https://doi.org/10.4095/321379. Open File 8648.

Kabanov, P., Vandenberg, R., Pelchat, P., Cameron, M., Dewing, K., 2020. Lithostratigraphy of Devonian basinal mudrocks in frontier areas of northwestern Canada augmented with ED-XRF technique. Arktos. https://doi.org/10.1007/s41063-020-00074-z. In press.

Kidder, D.L., Worsley, T.R., 2010. Phanerozoic large Igneous Provinces (LIPs), HEATT (Haline Euxinic Acidic Thermal Transgression) episodes, and mass extinctions. Palaeogeogr. Palaeoclimatol. Palaeoecol. 295, 162–191. https://doi.org/10.1016/j.palaeo.2010.05.036.

Kidder, D.L., Worsley, T.R., 2012. A human-induced hothouse climate? GSA Today 22, 4–11. https://doi.org/10.1130/G131A.1.

Klemme, H.D., Ulmishek, G.F., 1991. Effective petroleum source rocks of the world: stratigraphic distribution and controlling depositional factors. AAPG Bull. 75, 1809–1851. https://doi.org/10.1306/0C9B2A47-1710-11D7-8645000102C1865D.

Knapp, L.J., McMillan, J.M., Harris, N.B., 2017. A depositional model for organic-rich Duvernay Formation mudstones. Sediment. Geol. 347, 160–182. https://doi.org/10.1016/j.sedgeo.2016.11.012.

Koopmans, M.P., Köster, J., van Kaam-Peters, H.M.E., Kenig, F., Schouten, S., Hartgers, W.A., de Leeuw, J.W., Sinninghe Damsté, J.S., 1996. Diagenetic and catagenetic products of isorenieratene; molecular indicators for photic zone anoxia. Geochim. Cosmochim. Acta 60, 4467–4496. https://doi.org/10.1016/S0016-7037(96)00238-4.

Kravchinsky, V.A., 2012. Paleozoic large igneous provinces of Northern Eurasia: correlation with mass extinction events. Glob. Planet. Chang. 86–87, 31–36. https://doi.org/10.1016/j.gloplacha.2012.01.007.

Lane, L.S., 2007. Devonian–Carboniferous paleogeography and orogenesis, northern Yukon and adjacent Arctic Alaska. Can. J. Earth Sci. 44, 679–694. https://doi.org/10.1139/e06-131.

Lash, G.G., 2019. A global biogeochemical perturbation during the Middle Frasnian punctata event: evidence from muted carbon isotope signature in the Appalachian Basin, New York State (USA). Glob. Planet. Chang. 177, 239–254. https://doi.org/10.1016/j.gloplacha.2019.01.006.

Levin, L.A., 2003. Oxygen minimum zone benthos: adaptation and community response to hypoxia. Oceanogr. Mar. Biol. Annu. Rev. 41, 1–45.

Levman, B.G., von Bitter, P.H., 2002. The Frasnian–Famennian (mid–Late Devonian) boundary in the type section of the Long Rapids Formation, James Bay Lowlands, northern Ontario. Can. J. Earth Sci. 39, 1795–1818. https://doi.org/10.1139/E02-073.

Loenarz, C., Coleman, M.L., Boleininger, A., Schierwater, B., Holland, P.W., Ratcliffe, P.J., Schofield, C.J., 2011. The hypoxia-inducible transcription factor pathway regulates oxygen sensing in the simplest animal, Trichoplax adhaerens. EMBO Rep. 12, 63–70. https://doi.org/10.1038/embor.2010.170.

Lomnitz, U., Sommer, S., Dale, A.W., Löscher, C.R., Noffke, A., Wallmann, K., Hensen, C., 2015. Benthic phosphorus cycling in the Peruvian oxygen minimum zone. Biogeosciences. 13, 1367–1386. https://doi.org/10.5194/bg-13-1367-2016.

Mackenzie, W.C., 1973. Upper Devonian echinoderm debris beds with graded texture, District of Mackenzie, Northwest Territories. Can. J. Earth Sci. 10, 519–528. https://doi.org/10.1139/e73-051.

Magnall, J.M., Gleeson, S.A., Poulton, S.W., Gordon, G.W., Paradis, S., 2018. Links between seawater paleoredox and the formation of sediment-hosted massive sulphide (SHMS) deposits – Fe speciation and Mo isotope constraints from Late Devonian mudstones. Chem. Geol. 490, 45–60. https://doi.org/10.1016/j.chemgeo.2018.05.005.

Martinez, A.M., Boyer, D.L., Droser, M.L., Barrie, C., Love, G.D., 2019. A stable and productive marine microbial community was sustained through the end-Devonian Hangenberg Crisis within the Cleveland Shale of the Appalachian Basin, United States. Geobiology. 17, 27–42. https://doi.org/10.1111/gbi.12314.

Marynowski, L., Filipiak, P., 2007. Water column euxinia and wildfire evidence during deposition of the Upper Famennian Hangenberg event horizon from the Holy Cross Mountains (central Poland). Geol. Mag. 144, 569–595. https://doi.org/10.1017/S0016756807003317.

Marynowski, L., Filipiak, P., Pisarzovska, A., 2008. Organic geochemistry and palynofacies of the Early–Middle Frasnian transition (Late Devonian) of the Holy Cross Mountains, Southern Poland. Palaeogeogr. Palaeoclimatol. Palaeoecol. 268, 152–165. https://doi.org/10.1016/j.palaeo.2008.04.033.

Marynowski, L., Rakociński, M., Borcuch, E., Kremer, B., Schubert, B.A., Jahren, A.H., 2011. Molecular and petrographic indicators of redox conditions and bacterial communities after F/F mass extinction. Palaeogeogr. Palaeoclimatol. Palaeoecol. 306, 1–14. https://doi.org/10.1016/j.palaeo.2011.03.018.

Marynowski, L., Zatoń, M., Rakociński, M., Filipiak, P., Kurkiewicz, S., Pearce, T.J., 2012. Deciphering the upper Famennian Hangenberg Black Shale depositional environments based on multi-proxy record. Palaeogeogr. Palaeoclimatol. Palaeoecol. 346–347, 66–86. https://doi.org/10.1016/j.palaeo.2012.05.020.

McClung, W.S., Eriksson, K.A., Terry Jr., D.O., Cuffey, C.A., 2013. Sequence stratigraphic hierarchy of the Upper Devonian Foreknobs Formation, central Appalachian Basin, USA: evidence for transitional greenhouse to icehouse conditions. Palaeogeogr. Palaeoclimatol. Palaeoecol. 387, 104–125. https://doi.org/10.1016/j.palaeo.2013.07.020.

McClung, W.S., Cuffey, C.A., Eriksson, K.A., Terry Jr., D.O., 2016. An incised valley fill and lowstand wedges in the Upper Devonian Foreknobs Formation, central Appalachian Basin: implications for Famennian glacioeustasy. Palaeogeogr. Palaeoclimatol. Palaeoecol. 446, 125–143. https://doi.org/10.1016/j.palaeo.2016.01.014.

McGhee Jr., G.R., Clapham, M.E., Sheehan, P.M., Bpttjer, D.J., Droser, M.L., 2013. A new ecological-severity ranking of major Phanerozoic biodiversity crises. Palaeogeogr. Palaeoclimatol. Palaeoecol. 370, 260–270. https://doi.org/10.1016/j.palaeo.2012.12.019.

Meijer Drees, N.G., 1993. The Devonian succession in the subsurface of the Great Slave and Great Bear Plains, Northwest Territories. Geol. Surv. Can. Bull. 393https://doi.org/10.4095/183905. 222 p.

Melott, A.L., Bambach, R.K., 2014. Analysis of periodicity of extinction using the 2012 geological timescale. Paleobiology. 40, 177–196. https://doi.org/10.1666/13047.

Meyer, K.M., Kump, L.R., 2008. Oceanic euxinia in Earth history: causes and consequences. Annu. Rev. Earth Planet. Sci. 36, 251–288. https://doi.org/10.1146/annurev.earth.36.031207.124256.

Meyers, P.A., 2014. Why are the $\delta^{13}C_{org}$ values in Phanerozoic black shales more negative than in modern marine organic matter? Geochem. Geophys. Geosyst. 15, 3085–3106.

https://doi.org/10.1002/2014GC005305.
Mills, D.B., Ward, L.M., Jones, C., Sweeten, B., Forth, M., Treusch, A.H., Canfield, D.E., 2014. Oxygen requirements of the earliest animals. PNAS. 111, 4168–4172. https://doi.org/10.1073/pnas.1400547111.
Mills, D.B., Francis, W.R., Vargas, S., Larsen, M., Elmans, C.P.H., Canfield, D.E., Wörheide, G., 2018. The last common ancestor of animals lacked the HIF pathway and respired in low-oxygen environments. eLife. 7https://doi.org/10.7554/eLife.31176. 17 p.
Mosch, T., Sommer, S., Dengler, M., Noffke, A., Bohlen, L., Pfannkuche, O., Liebetrau, V., Wallmann, K., 2012. Factors influencing the distribution of epibenthic megafauna across the Peruvian oxygen minimum zone. Deep Sea Res. I. Oceanogr. Res. Pap. 68, 123–135. https://doi.org/10.1016/j.dsr.2012.04.014.
Muir, I., Wong, P., Wendte, J., 1984. Devonian Hare Indian – Ramparts (Kee Scarp) evolution, Mackenzie Mountains and subsurface Norman Wells, N.W.T.: Basin-fill and platform development. In: Eliuk, L., Kaldi, J., Watts, N. (Eds.), Carbonates in Subsurface and Outcrop. Can. Soc. Petrol. Geol. Core Conference, pp. 82–102.
Muir, I., Dixon, O.A., 1985. Devonian Hare Indian-Ramparts evolution, Mackenzie Mountains, NWT, basin-fill and platform-reef development. In: Brophy, J.A. (Ed.), Contributions to the Geology of the Northwest Territories. 2. pp. 85–90.
Narkiewicz, M., 2007. Development and inversion of Devonian and Carboniferous basins in the eastern part of the Variscan.foreland (Poland). Geol. Q. 51, 231–256. https://gq.pgi.gov.pl/article/view/7453 Accessed March 02, 2020.
Narkiewicz, K., Bultynck, P., 2007. Conodont biostratigraphy of shallow marine Givetian deposits from the Radom–Lublin area (SE Poland). Geol. Q. 51, 419–442. https://gq.pgi.gov.pl/article/view/7466 Accessed March 02, 2020.
Nelson, J.L., Colpron, M., Israel, S., 2013. Chapter 3. The Cordillera of British Columbia, Yukon, and Alaska: Tectonics and Metallogeny. In: Colpron, M., Bissig, T., Rusk, B.G., Thompson, J.F.H. (Eds.), Tectonics, Metallogeny, and Discovery: The North American Cordillera and Similar Accretionary Settings. Society of Economic Geologists, Special Publication. 17pp. 53–109.
Nicoll, R.S., 1984. Conodont distribution in the marginal slope facies of the Upper Devonian reef complex, Canning Basin, Western Australia. In: Clark, D.L. (Ed.), Conodont Biofacies and Provincialism. 196. Geological Society of America, Special Paper, pp. 127–141. https://doi.org/10.1130/SPE196-p127.
Oehlert, A.M., Swart, P.K., Eberli, G.P., Evans, S., Frank, T.D., 2019. Multi-proxy constraints on the significance of covariant $\delta^{13}C$ values in carbonate and organic carbon during the early Mississippian. Sedimentology 66, 241–261. https://doi.org/10.1111/sed.12502.
Patruno, S., Helland-Hansen, W., 2018. Clinoforms and clinoform systems: review and dynamic classification scheme for shorelines, subaqueous deltas, shelf edges and continental margins. Earth Sci. Rev. 185, 202–233. https://doi.org/10.1016/j.earscirev.2018.05.016.
Percival, L.M.E., Selby, D., Bond, D.P.G., Rakociński, M., Racki, G., Marynowski, L., Adatte, T., Spangenberg, J.E., Föllmi, K.B., 2019. Pulses of enhanced continental weathering associated with multiple Late Devonian climate perturbations: evidence from osmium-isotope compositions. Palaeogeogr. Palaeoclimatol. Palaeoecol. 524, 240–249. https://doi.org/10.1016/j.palaeo.2019.03.036.
Percival, L.M.E., Bond, D.P.G., Rakociński, M., Marynowski, L., Hood, A.V.S., Adatte, T., Spangenberg, J.E., Föllmi, K.B., 2020. Phosphorus-cycle disturbances during the Late Devonian anoxic events. Glob. Planet. Chang. 184. https://doi.org/10.1016/j.gloplacha.2019.103070.
Philp, R.P., DeGarmo, C.D., 2020. Geochemical characterization of the Devonian-Mississippian Woodford Shale from the McAlister Cemetery Quarry, Criner Hills Uplift, Ardmore Basin, Oklahoma. Mar. Pet. Geol. 112, 104078. https://doi.org/10.1016/j.marpetgeo.2019.104078.
Piecuch, C.G., Ponte, R.M., 2014. Mechanisms of global-mean steric sea level change. J. Clim. 27, 824–834. https://doi.org/10.1175/JCLI-D-13-00373.1.
Pisarzowska, A., Racki, G., 2012. Isotopic chemostratigraphy across the Early–Middle Frasnian transition (Late Devonian) on the South Polish carbonate shelf: a reference for the global punctata event. Chem. Geol. 334, 199–220. https://doi.org/10.1016/j.chemgeo.2012.10.034.
Pisera, A., 2006. Palaeontology of sponges – a review. Can. J. Zool. 84, 242–261. https://doi.org/10.1139/z05-169.
Playford, P.E., 1980. Devonian “Great Barrier Reef” of canning basin, Western Australia. AAPG Bull. 64, 814–840. https://doi.org/10.1306/2F9193BE-16CE-11D7-8645000102C1865D.
Pugh, D.C., 1983. Pre-Mesozoic geology in the subsurface of Peel River Map area. In: Yukon Territory and District of Mackenzie. Geological Survey of Canada Memoir. 401, https://doi.org/10.4095/119498. 61p.
Pugh, D.C., 1993. Subsurface geology and pre-Mesozoic strata. In: Great Bear River map area, District of Mackenzie, Geological Survey of Canada, Memoir 430, https://doi.org/10.4095/183985. 137 p.
Pyle, L.J., Gal, L.P., 2016. Reference Section for the Horn River Group and Definition of the Bell Creek Member, Hare Indian Formation in central Northwest Territories. Bull. Can. Petrol. Geol. 64, 67–98. https://doi.org/10.2113/gscpgbull.64.1.67.
Pyle, L.J., Gal, L.P., Hadlari, T., 2015. Thermal maturity trends for Devonian Horn River Group units and equivalent strata in the Mackenzie Corridor, Northwest Territories and Yukon. Geol. Surv. Can. Open File 7850. https://doi.org/10.4095/296446.
Racki, G., 2005. Toward understanding Late Devonian global events; few answers, many questions. In: Over, D.J., Morrow, J.R., Wignall, P.B. (Eds.), Understanding Late Devonian and Permian-Triassic Biotic and Climatic Events: Towards an Integrated Approach. Developments in Palaeontology and Stratigraphy. Vol. 20. pp. 5–36 eBook ISBN: 9780080457840.
Racki, G., 2020. Volcanic scenario of the Frasnian–Famennian major biotic crisis and other Late Devonian global changes: more answers than questions? Glob. Planet. Chang In press.
Racki, G., Racka, M., Matyja, H., Devleeschouwer, X., 2002. The Frasnian/Famennian boundary interval in the South Polish-Moravian shelf basins: integrated event-stratigraphical approach. Palaeogeogr. Palaeoclimatol. Palaeoecol. 181, 251–297. https://doi.org/10.1016/S0031-0182(01)00481-3.
Racki, G., Rakociński, M., Marynowski, L., Wignall, P.B., 2018. Mercury enrichments and the Frasnian-Famennian biotic crisis: a volcanic trigger proved? Geology 46, 543–546. https://doi.org/10.1130/G40233.1.
Ray, D.C., van Buchem, F.S.P., Baines, G., Dacies, A., Gréselle, B., Simmons, M.D., Robson, C., 2020. The magnitude and cause of short-term eustatic cretaceous sea-level change: a synthesis. Earth Sci. Rev. 197, 102901. https://doi.org/10.1016/j.earscirev.2019.102901.
Reolid, M., 2014. Pyritized radiolarians and siliceous sponges from oxygen-restricted deposits (Lower Toarcian, Jurassic). Facies 60, 789–799. https://doi.org/10.1007/s10347-014-0404-6.
Requejo, A.G., Allan, J., Creaney, S., Gray, N.R., Cole, K.S., 1992. Aryl isoprenoids and diaromatic carotenoids in Paleozoic source rocks and oils from the Western Canada and Williston Basins. Org. Geochem. 19, 245–264. https://doi.org/10.1016/0146-6380(92)90041-U.
Retallack, G.J., Huang, C., 2011. Ecology and evolution of Devonian trees in New York, USA. Palaeogeogr. Palaeoclimatol. Palaeoecol. 29, 110–128. https://doi.org/10.1016/j.palaeo.2010.10.040.
Riboulleau, A., Spina, A., Vecoli, M., Riquier, L., Quijada, M., Tribovillard, N., Averbuch, O., 2018. Organic matter deposition in the Ghadames Basin (Libya) during the Late Devonian—a multidisciplinary approach. Palaeogeogr. Palaeoclimatol. Palaeoecol. 497, 37–51. https://doi.org/10.1016/j.palaeo.2018.02.004.
Rich, J.L., 1951. Three critical environments of deposition and criteria for recognition of rocks deposited in each of them. GSA Bull. 62, 1–20.
Richter, D.K., Neuser, R.D., Schreuer, J., Gies, H., Immenhauser, A., 2011. Radiaxial-fibrous calcites: a new look at an old problem. Sediment. Geol. 239, 23–36. https://doi.org/10.1016/j.sedgeo.2011.06.003.
Saltzman, M.R., Thomas, E., 2012. Chapter 11. Carbon isotope stratigraphy. In: Gradstein, F., Ogg, J., Schmitz, M.D., Ogg, G. (Eds.), The Geologic Time Scale 2012. Elsevier, pp. 207–232. https://doi.org/10.1016/B978-0-444-59425-9.00011-1.
Sames, B., Wagreich, M., Wendler, J.E., Haq, B.U., Conrad, C.P., Melinte-Dobrinescu, M.C., Hug, X., Wendler, I., Wolfgring, E., Yilmaz, I.Ö., Zorina, S.O., 2016. Review: short-term sea-level changes in a greenhouse world – a view from the cretaceous. Palaeogeogr. Palaeoclimatol. Palaeoecol. 441, 393–411. https://doi.org/10.1016/j.palaeo.2015.10.045.
Sames, B., Wagreich, M., Conrad, C.P., Iqbal, S., 2020. Aquifer-eustasy as the main driver of short-term sea-level fluctuations during Cretaceous hothouse climate phases. Geol. Soc. Lond., Spec. Publ. 498. https://doi.org/10.1144/SP498-2019-105.
Sandberg, C.A., Morrow, J.R., Ziegler, W., 2002. Late Devonian sea-level changes, catastrophic events, and mass extinctions. In: Koeberl, C., MacLeod, K.G. (Eds.), Catastrophic Events and Mass Extinctions: Impacts and beyond. Geological Society of America Special Paper. 356pp. 473–487. https://doi.org/10.1130/0-8137-2356-6.473.
Schlager, W., 1989. Drowning unconformities on carbonate platforms. In: Crevello, P.D., Wilson, J.L., Sarg, J.F., Read, J.F. (Eds.), Controls on Carbonate Platform and Basin Development. Society of Economic Paleontologists and Mineralogists Special Publication. 41pp. 15–25.
Schlager, W., 2005. Carbonate sedimentology and sequence stratigraphy. SEPM Concepts Sedimentol. Paleontol. 8https://doi.org/10.2110/csp.05.08. 209 p.
Scholz, F., Siebert, C., Dale, A.W., Frank, M., 2017. Intense molybdenum accumulation in sediment underneath a nitrogenous water column and implications for the reconstruction of paleo-redox conditions based on molybdenum isotopes. Geochim. Cosmochim. Acta. 213, 400–417. https://doi.org/10.1016/j.gca.2017.06.048.
Sinninghe Damste, J.S., Kenig, F., Koopmans, M.P., Koster, J., Schouten, S., Hayes, J.M., de Leeuw, J.W., 1995. Evidence for gammacerane as an indicator of water column stratification. Geochim. Cosmochim. Acta 59, 1895–1900. https://doi.org/10.1016/0016-7037(95)00073-9.
Śliwiński, M.G., Whalen, M.T., Newberry, R.J., Payne, J.H., Day, J.E., 2011. Stable isotope ($\delta^{13}C_{carb\ and\ org}$, $\delta^{15}N_{org}$) and trace element anomalies during the Late Devonian ‘punctata Event’ in the Western Canada Sedimentary Basin. Palaeogeogr. Palaeoclimatol. Palaeoecol. 307, 245–271. https://doi.org/10.1016/j.palaeo.2011.05.024.
Smith, L.B., Schieber, J., Wilson, R.D., 2019. Shallow-water onlap model for the deposition of Devonian black shales in New York, USA. Geology 47, 279–283. https://doi.org/10.1130/G45569.1.
Smith, L.B., Schieber, J., Wilson, R.D., 2020. Shallow-water onlap model for the deposition of Devonian black shales in New York, USA: Reply. Geology 47. e496. https://doi.org/10.1130/G47057Y.1.
Soreghan, G.S., Giles, K.A., 1999. Amplitudes of Late Pennsylvanian glacioeustasy. Geology 27, 255–258. https://doi.org/10.1130/0091-7613(1999)027<0255:AOLPG>2.3.CO;2.
Spaak, G., Edwards, D.S., Allen, H.J., Grotheera, H., Summons, R.E., Coolen, M.J.L., Grice, K., 2018. Extent and persistence of photic zone euxinia in Middle–Late Devonian seas – insights from the Canning Basin and implications for petroleum source rock formation. Mar. Pet. Geol. 93, 33–56. https://doi.org/10.1016/j.marpetgeo.2018.02.033.
Stanton Jr., R.J., Jeffery, D.L., Guillemette, R.N., 2000. Oxygen minimum zone and internal waves as potential controls on location and growth of waulsortian mounds (Mississippian, Sacramento Mountains, New Mexico). Facies 42, 161–176.
Steel, R.J., Olsen, T., 2002. Clinoforms, clinoform trajectory and deepwater sands. In: Armentrout, J.M., Rosen, N.C. (Eds.), Sequence Stratigraphic Models for Exploration and Production: Evolving Methodology, Emerging Models and Application Histories. GCS-SEPM Special Publication, pp. 367–381. https://doi.org/10.5724/gcs.02.22.

0367.
Stoakes, F.A., 1980. Nature and control of shale basin fill and its effect on reef growth and termination: Upper Devonian, Duvernay and Ireton Formations of Alberta, Canada. Can. Soc. Pet. Geol. Bull. 28, 345–410.
Summons, R.E., Powell, T.G., 1987. Identification of aryl isoprenoids in source rocks and crude oils: biological markers for the green sulphur bacteria. Geochim. Cosmochim. Acta 51, 557–566. https://doi.org/10.1016/0016-7037(87)90069-X.
Tribovillard, N., Algeo, T.J., Baudin, F., Riboulleau, A., 2012. Analysis of marine environmental conditions based on molybdenum–uranium covariation—applications to Mesozoic paleoceanography. Chem. Geol. 324–325, 46–58. https://doi.org/10.1016/j.chemgeo.2011.09.009.
Tribovillard, N., Algeo, T., Lyons, T.W., Riboulleau, A., 2006. Trace metals as paleoredox and paleoproductivity proxies: an update. Chem. Geol. 232, 12–32. https://doi.org/10.1016/j.chemgeo.2006.02.012.
Tyson, R.V., Pearson, T.H., 1991. Modern and ancient continental shelf anoxia: an overview. In: Tyson, R.V., Pearson, T.H. (Eds.), Modern and Ancient Continental Shelf Anoxia. Geological Society, London, Special Publications. 58pp. 1–26. https://doi.org/10.1144/GSL.SP.1991.058.01.01.
Van Hengstum, P.J., Gröcke, D.R., 2008. Stable isotope record of the Eifelian-Givetian boundary Kačák-otomari Event (Middle Devonian) from Hungry Hollow, Ontario, Canada. Can. J. Earth Sci. 45, 353–366. https://doi.org/10.1139/E08-005.
Ver Straeten, C.A., Brett, C.B., Sageman, B.B., 2011. Mudrock sequence stratigraphy: a multi-proxy (sedimentological, paleobiological and geochemical) approach, Devonian Appalachian Basin. Palaeogeogr. Palaeoclimatol. Palaeoecol. 304, 54–73. https://doi.org/10.1016/j.palaeo.2010.10.010.
Ver Straeten, C., Brett, C., Baird, G., Boyer, D., Lindemann, R., Ivany, L., Over, D.J., Witzke, B., 2020. Shallow-water onlap model for the deposition of Devonian black shales in New York, USA: comment. Geology 47, e495. https://doi.org/10.1130/G46928C.1.
Vierek, A., 2014. Small-scale cyclic deposition in the Frasnian (Upper Devonian) of the Holy Cross Mountains, Poland. Geologos 20, 239–258. https://doi.org/10.2478/logos-2014-0019.
Vishnevskaya, V., Pisera, A., Racki, G., 2002. Siliceous biota (radiolarians and sponges) and the Late Devonian biotic crisis: the Polish reference. Acta Palaeontol. Pol. 47, 211–226 http://www.paleo.pan.pl/acta/acta47/app47 – 211.pdf. Accessed March 02, 2020.
Wagreich, M., Lein, R., Sames, B., 2014. Eustasy, its controlling factors, and the limnoeustatic hypothesis – concepts inspired by Eduard Suess. Austrian J. Earth Sci. 107, 115–131. https://www.univie.ac.at/ajes/archive/volume_107_1/ Accessed March 02, 2020.
Wendte, J., Uyeno, T., 2005. Sequence stratigraphy and evolution of Middle to Upper Devonian Beaverhill Lake strata, south-Central Alberta. Bull. Can. Petrol. Geol. 53, 250–354. https://doi.org/10.2113/53.3.250.
Witzke, B.J., Bunker, B.J., 1996. Relative sea-level changes during Middle Ordovician through Mississippian deposition in the Iowa area, North American craton. In: Witzke, B.J., Ludvigson, G.A., Day, J. (Eds.), Paleozoic Sequence Stratigraphy: Views from the North American Craton. Geological Society of America Special Paper 306pp. 307–330. https://doi.org/10.1130/0-8137-2306-X.307.
Yans, J., Corfield, R.M., Racki, G., Préat, A., 2007. Evidence for major perturbation of carbon cycle in the Middle Frasnian punctata conodont Zone. Geol. Mag. 144, 263–270. https://doi.org/10.1017/S0016756806003037.
Yose, L.A., Brown, S., Davis, T.L., Eiben, T., Kompanik, G.S., Maxwell, S.R., 2001. 3-D geologic model of a fractured carbonate reservoir, Norman Wells Field, NWT, Canada. Bull. Can. Petrol. Geol. https://doi.org/10.2113/49.1.86.
Zhang, X., Joachimski, M.M., Over, D.J., Maa, K., Huang, C., Gonga, Y., 2019. Late Devonian carbon isotope chemostratigraphy: a new record from the offshore facies of South China. Glob. Planet. Chang. 182. https://doi.org/10.1016/j.gloplacha.2019.103024.